

Asymptotic Analysis of Shallow Water Moment Equations

Mieke Daemen¹, Julio Careaga¹, Zhenning Cai², and Julian Koellermeier^{1,3}

¹ Bernoulli Institute, University of Groningen, Nijenborgh 9, Groningen, 9747 AG, The Netherlands

² Department of Mathematics, National University of Singapore, 10 Lower Kent Ridge Road, Singapore 119076, Singapore

³ Department of Mathematics, Computer Science and Statistics, Ghent University, Krijgslaan 281-S9, Ghent, 9000, Belgium

Abstract

The Shallow Water Moment Equations (SWME) are an extension of the Shallow Water Equations (SWE) for improved modelling of free-surface flows. In contrast to the SWE, the SWME incorporate vertical velocity profile information. The SWME framework approximates vertical velocity profiles using a polynomial expansion with Legendre polynomials and polynomial coefficients, also called moment variables. The SWME have an increased number of variables that must always be incorporated, even when the flow approaches a viscous slip equilibrium state that could be characterised by vanishing moment variables. To reduce the complexity of the SWME in cases proximate to this equilibrium, we conduct an asymptotic analysis of the SWME. This yields the closed form Reduced Shallow Water Moment Equations (RSWME) for deviations from the equilibrium. The RSWME have fewer variables, compared to the SWME. The hyperbolicity of the RSWME is analysed. Numerical tests include a wave with a sharp height gradient, a smoother height gradient and a square root velocity profile. The numerical tests demonstrate that the RSWME reduce computational cost up to 77% compared to the SWME and improves accuracy up to 88% over the SWE.

Keywords: shallow free-surface flows, Chapman Enskog expansion, shallow water moment equations

MSC 2020: 35L60, 76D05, 35C20

1 Introduction

The Shallow Water Equations (SWE) are widely applied to model free-surface flows in contexts such as ocean modelling [16] and snow avalanche simulation [17]. These equations result from depth-averaging the Navier–Stokes equations, assuming a simplified vertical velocity profile represented by the depth-averaged velocity [21]. A significant limitation of this approach is the inability to model the detailed evolution of vertical structure, which can lead to modelling errors in scenarios with non-uniform vertical velocity profiles such as tsunami propagation [1] or dam-break flows [14]. Furthermore, in the presence of bottom friction, vertical velocity profiles become non-uniform. As a result, applying the SWE introduces errors, especially in sediment transport scenarios [7]. Hence, the SWE are insufficient for modelling non-uniform vertical velocity profiles. As a possible remedy, the Shallow Water Moment Equations (SWME) have been derived to approximate vertical velocity profiles within a model for shallow flows [12].

Within the SWME framework, vertical velocity profiles are approximated by expanding them in Legendre polynomials, with the expansion coefficients referred to as moment variables. In [12], the SWME are derived from the incompressible hydrostatic Navier-Stokes equations. The derivation employs the method of moments, where the horizontal velocity is expanded in vertical direction using a Legendre polynomial basis, and a Galerkin projection is then applied to derive the evolution equations for the moment coefficients.

Subsequently, the moment model concept was also applied to non-hydrostatic cases [18], non-Newtonian cases with sediment transport [7], and two-dimensional radially symmetric free-surface flows [20]. Additionally, as discussed in [2], the two-dimensional SWME are analysed, focussing on their mathematical structure. In [12, 18, 20], it was shown that increasing the number of moments yields solutions that more closely approximate reference solutions computed via a direct discretisation of the Navier-Stokes equations, particularly when compared to the SWE. Thus, the SWME offer a clear advantage in enhancing the accuracy of free-surface flow models.

In [11], it has been demonstrated that for specific cases, the eigenvalues of the transport matrix exhibit non-zero imaginary components. Consequently, the propagation speeds in the SWME system are no longer real and instabilities can occur. To address this loss of hyperbolicity, the SWME transport matrix is linearised around a linear velocity profile resulting in the Hyperbolic Shallow Water Moment Equations (HSWME) [11]. Additionally, the Shallow Water Linearised Moment Equations (SWLME) provide an alternative hyperbolic model by omitting non-linear terms in the SWME-system [10].

The SWME, HSWME, and SWLME incorporate more variables than the SWE, making these moment models computationally more expensive. This increase arises because the SWME, HSWME, and SWLME each incorporate additional moment variables, rather than only fluid height and averaged velocity variables. To mitigate this increase in computational expense, we aim to develop a method to reduce the number of variables in the SWME. To achieve this reduction, the friction term must be considered, as it determines which model variables can be simplified through an appropriate closure.

We must therefore consider not only the transport component of the SWME but also the source term. The model in [12] considers the simple case of a Newtonian friction term with viscosity and slip length parameters. In the SWME, this source-term accounts for both viscous dissipation inside the water and boundary effects at the fluid-solid interface.

In [8], the equilibria and stability of the hyperbolic HSWME and SWLME models are analysed, focussing on the influence of the slip length parameter in the source term. These models exhibit three distinct equilibrium manifolds, each characterised by specific source-term behaviour: (1) a water-at-rest state for finite viscosity and slip length, (2) a constant-velocity state when the slip length significantly exceeds the fluid height, and (3) a bottom-at-rest state when the slip length is much smaller than the fluid height. Through structural stability analysis and numerical simulations in [8], the water-at-rest and constant-velocity equilibria were shown to be stable, whereas the bottom-at-rest equilibrium could exhibit instability.

The constant-velocity equilibrium state of the original SWME system from [12] can be described without the additional polynomial coefficients that the SWME are solving for. When simulating perturbations from this equilibrium, the full SWME model incurs potentially high computational costs to resolve the small vertical variations in the form of the polynomial coefficients. On the other hand, a computationally faster SWE model fails to capture these variations because it relies solely on average velocity and fluid height. To balance runtime and accuracy, we aim to derive efficient approximate solutions near equilibria, so that solving a potentially large system for the polynomial coefficients is not necessary. These approximations emerge from systematically applying asymptotic analysis to the SWME for various scalings of the viscosity and the slip length.

For the asymptotic analysis a technique similar to Chapman Enskog expansion in kinetic theory from [6] will be applied to the SWME with scalings of the slip length and viscosity friction parameters. For similar approaches applied to the Boltzmann Equations with various scalings of the non-dimensional Knudsen number, we refer to [3, 13, 19].

Applying asymptotic expansions and deriving explicit closure relations for the higher-order terms reduces the numbers of variables in the SWME, yielding the Reduced Shallow Water Moment Equations (RSWME). This derivation process consists of substituting asymptotic expansions into the governing equations and performing an order-of-magnitude analysis to isolate the dominant terms. Deriving analytical expressions for a subset of the variables in terms of the remaining model variables and substituting them back into the SWME ultimately yields a closed system. We derive the RSWME up to an arbitrary order of moments. We show that the closed RSWME system is identical for large numbers of moments. Thus, numerical solutions for varying numbers of moments can be obtained by solving the same system of partial differential equations, significantly reducing computational cost to simulate free-surface flows near equilibrium with varying numbers of moments.

Additionally, for an arbitrary number of moments the hyperbolicity of the RSWME is analysed, and a hyperbolic regularisation procedure is developed. Numerical tests show that the new RSWME lead to a higher accuracy compared to the standard SWE, and a higher computational efficiency than the full SWME for flows close to equilibrium.

The rest of this paper is structured as follows: Section 2 presents the SWME system and derives asymptotic approximations for varying scalings of the viscosity and slip length parameters. In Section 3, the Chapman–Enskog expansion method is applied to a viscous slip scenario, resulting in the RSWME through the dimensional reduction of the SWME system. Subsequently, a hyperbolicity analysis of the RSWME is performed. Section 4 then presents numerical tests for smooth wave scenarios. Finally, Section 5 concludes the paper, summarising the key findings.

2 Shallow Water Moment Equations

This section briefly presents the derivation of the SWE and SWME models based on [12]. The SWE and SWME systems are derived from the incompressible Navier-Stokes Equations (NSE).

2.1 Shallow water model

The Shallow Water Equations (SWE) are a set of hyperbolic partial differential equations that describe the behaviour of free-surface flows where horizontal length-scales significantly exceed vertical ones. The SWE are derived by depth-integrating the NSE.

The classical SWE for a water column of fluid height h and depth-averaged velocity u_m in the horizontal direction x are

$$\begin{aligned} \partial_t h + \partial_x(hu_m) &= 0, \\ \partial_t(hu_m) + \partial_x\left(hu_m^2 + \frac{gh^2}{2}\right) + gh\partial_x(h_b) &= -\frac{\nu}{\lambda}u_m, \end{aligned} \quad (1)$$

where ν and λ denote viscosity and slip length, respectively. The bottom height is given by h_b . The right-hand side term of (1) represents the bottom slip penalty.

The SWE from (1) provide a computationally efficient two-variable system for flow modelling through depth-averaging. However, depth-averaging leads to errors in cases where significant horizontal velocity variations occur [12].

2.2 Deriving SWME from the Navier–Stokes equations

This subsection presents the derivation of the SWME, as introduced in [12], where vertical velocity profiles are approximated using a polynomial expansion to account for vertical flow structure.

To obtain the SWME system, we transform the NSE through the following two steps: (1) mapping the vertical coordinate z , and (2) applying a polynomial Legendre expansion to velocity variables.

Vertical coordinate mapping As presented in [12], a coordinate mapping is employed to enable a more efficient representation of horizontal velocity variations along the vertical axis. This mapping normalises the vertical coordinate z , between the bottom fluid height $z = h_b(x, t)$ and the free-surface fluid height $z = h_s(x, t)$ as

$$\zeta(x, t, z) = \frac{z - h_b(x, t)}{h(x, t)}, \quad (2)$$

where $h(x, t) = h_b(x, t) - h_s(x, t)$ is the fluid height. The mapped vertical coordinate ζ from (2) is defined within the interval $[0, 1]$. As a result, the z -coordinate, $z \in [h_b(x, t), h_s(x, t)]$, is mapped to a normalised domain $\zeta(x, t): \mathbb{R} \times [0, T] \rightarrow [0, 1]$.

Polynomial expansion In the second step, [12] expands the horizontal velocity variable $u(x, t, \zeta)$ in the vertical direction ζ using a polynomial expansion centred around the depth-averaged velocity $u_m(x, t)$. The velocity $u(x, t, \zeta): \mathbb{R} \times [0, T] \times [0, 1] \rightarrow \mathbb{R}$ is expressed as

$$u(x, t, \zeta) = u_m(x, t) + \sum_{j=1}^N \alpha_j(x, t) \phi_j(\zeta), \quad (3)$$

where $\alpha_j(x, t): \mathbb{R} \times [0, T] \rightarrow \mathbb{R}$ represents the expansion coefficients called moments, and $\phi_j: [0, 1] \rightarrow \mathbb{R}$ denotes the scaled Legendre polynomial of degree j for $j = 0, \dots, N$. These basis functions are normalised such that $\phi_j(0) = 1$ for $j = 1, \dots, N$. The scaled Legendre polynomials ϕ_j are

$$\phi_j(\zeta) = \frac{1}{j!} \frac{d^j}{d\zeta^j} (\zeta - \zeta^2)^j, \quad j = 1, \dots, N. \quad (4)$$

For example, the first two polynomials are

$$\phi_1(\zeta) = 1 - 2\zeta, \quad \phi_2(\zeta) = 1 - 6\zeta + 6\zeta^2. \quad (5)$$

The basis functions satisfy the orthogonality condition

$$\int_0^1 \phi_j(\zeta) \phi_k(\zeta) d\zeta = \frac{\delta_{jk}}{2k+1}, \quad (6)$$

where δ_{jk} is the Kronecker delta for all $j, k = 1, \dots, N$.

The orthogonality property (6) is essential to derive the SWME. This property leads to a separate time-derivative term for the i -th moment, thereby causing the nonlinear terms to couple the moment variables. As a result, the orthogonality property yields a sparse SWME where additional nonlinear terms do not appear in the time derivative.

In the expansion (3), the parameter $N \in \mathbb{N}$ determines the order of the polynomial approximation. Increasing N generally improves the representation of vertically complex flow behaviour [12], whereas setting $N = 0$ results in the classical depth-averaged SWE from (1).

After mapping the Navier-Stokes momentum equation in the z -direction and substituting the polynomial expansion formula from (3), the momentum equation is projected onto Legendre polynomials. Multiplying by ϕ_j and integrating over $\zeta \in [0, 1]$ yields differential equations for α_j ($j = 1, \dots, N$), while projecting onto $\phi_0 = 1$ gives the equation for u_m . The evolution equation for h is derived by depth-integrating the vertically mapped continuity equation. The resulting $N + 2$ equations for the variables $h, u_m, \alpha_1, \dots, \alpha_N$ are

$$\partial_t h + \partial_x(hu_m) = 0, \quad (7a)$$

$$\partial_t(hu_m) + \partial_x \left(h \left(u_m^2 + \sum_{j=1}^N \frac{\alpha_j^2}{2j+1} \right) + \frac{gh^2}{2} \right) = -\frac{\nu}{\lambda} \left(u_m + \sum_{j=1}^N \alpha_j \right) - gh \partial_x(h_b), \quad (7b)$$

$$\begin{aligned} \partial_t(h\alpha_i) + \partial_x \left(h \left(2u_m\alpha_i + \sum_{j,k=1}^N A_{ijk}\alpha_j\alpha_k \right) \right) &= u_m \partial_x(h\alpha_i) - \sum_{j,k=1}^N B_{ijk} \partial_x(h\alpha_j)\alpha_k \\ &\quad - (2i+1) \frac{\nu}{\lambda} \left(u_m + \sum_{j=1}^N \alpha_j + \frac{\lambda}{h} \sum_{j=1}^N C_{ij}\alpha_j \right), \end{aligned} \quad (7c)$$

for $i = 1, \dots, N$.

For simplicity, we assume uniform bathymetry, so $\partial_x(h_b) = 0$. The constants A_{ijk} , B_{ijk} , and C_{ij} for $i, j, k = 1, \dots, N$ denote integrals arising from scaled depth integration. These constants are given by

$$A_{ijk} = (2i+1) \int_0^1 \phi_i \phi_j \phi_k d\zeta, \quad (8)$$

$$B_{ijk} = (2i+1) \int_0^1 \partial_\zeta \phi_i \left(\int_0^\zeta \phi_j d\hat{\zeta} \right) \phi_k d\zeta, \quad (9)$$

$$C_{ij} = (2i+1) \int_0^1 \partial_\zeta \phi_i \partial_\zeta \phi_j d\zeta. \quad (10)$$

Closed-form SWME The SWME (7a)-(7c) can be expressed in matrix form as

$$\partial_t U + \frac{\partial F(U)}{\partial U} \partial_x U = Q(U) \partial_x U + S(U), \quad (11)$$

where $U = (h, hu_m, h\alpha_1, \dots, h\alpha_N) \in \mathbb{R}^{N+2}$. Here, the Jacobian of the conservative flux $\frac{\partial F(U)}{\partial U} \in \mathbb{R}^{(N+2) \times (N+2)}$ is defined as

$$\frac{\partial F(U)}{\partial U} = \begin{pmatrix} 0 & 1 & 0 & \dots & 0 \\ gh - u_m^2 - \sum_{i=1}^N \frac{\alpha_i}{2i+1} & 2u_m & \frac{2\alpha_1}{2 \cdot 1 + 1} & \dots & \frac{2\alpha_N}{2N+1} \\ -2u_m\alpha_1 - \sum_{j,k=1}^N A_{1jk}\alpha_j\alpha_k & 2\alpha_1 & 2u_m\delta_{11} + 2\sum_{k=1}^N A_{11k}\alpha_k & \dots & 2u_m\delta_{1N} + 2\sum_{k=1}^N A_{1Nk}\alpha_k \\ \vdots & \vdots & \vdots & \ddots & \vdots \\ -2u_m\alpha_N - \sum_{j,k=1}^N A_{Njk}\alpha_j\alpha_k & 2\alpha_N & 2u_m\delta_{N1} + 2\sum_{k=1}^N A_{N1k}\alpha_k & \dots & 2u_m\delta_{NN} + 2\sum_{k=1}^N A_{NNk}\alpha_k \end{pmatrix}.$$

The non-conservative term $Q(U) \in \mathbb{R}^{(N+2) \times (N+2)}$ is given by

$$Q(U) = \begin{pmatrix} 0 & 0 & 0 & \dots & 0 \\ 0 & 0 & 0 & \dots & 0 \\ 0 & 0 & u_m\delta_{11} + \sum_{k=1}^N B_{11k}\alpha_k & \dots & u_m\delta_{1N} + \sum_{k=1}^N B_{1Nk}\alpha_k \\ \vdots & \vdots & \vdots & \ddots & \vdots \\ 0 & 0 & u_m\delta_{N1} + \sum_{k=1}^N B_{N1k}\alpha_k & \dots & u_m\delta_{NN} + \sum_{k=1}^N B_{NNk}\alpha_k \end{pmatrix}.$$

The friction term $S(U) \in \mathbb{R}^{N+2}$ includes the Newtonian slip terms from [12] and is determined by

$$S_0(U) = 0, \quad S_1(U) = -\frac{\nu}{\lambda} \sum_{j=1}^N \alpha_j, \quad S_i(U) = -(2i+1) \frac{\nu}{\lambda} \sum_{j=1}^N \alpha_j - (2i+1) \frac{\nu}{h} \sum_{j=1}^N C_{ij} \alpha_j, \quad i = 2, \dots, N+2. \quad (12)$$

The system matrix $A(U) \in \mathbb{R}^{(N+2) \times (N+2)}$ is defined as

$$A(U) = \frac{\partial F(U)}{\partial U} - Q(U), \quad (13)$$

Consequently, the full system (11) is expressed as

$$\partial_t U + A(U) \partial_x U = S(U). \quad (14)$$

3 Asymptotic approximations of the SWME with viscous slip scaling

In this section we present asymptotic approximations of the SWME using Chapman Enskog expansion. To this end, we introduce a small positive parameter, $\varepsilon \ll 1$, and apply a scaling to the friction parameters, ν and λ in (12). We apply asymptotic expansions to the variables in the system (14), according to the expression

$$U_i = U_i^{(0)} + \varepsilon U_i^{(1)} + \varepsilon^2 U_i^{(2)} + \mathcal{O}(\varepsilon^3), \quad i = 1, \dots, N+2. \quad (15)$$

The values of the different magnitude coefficients $U_i^{(j)}$ for $i = 1, \dots, N+2$ and $j = 0, 1, 2$ are obtained by substituting (15) into (7a)-(7c) or equivalently (14) and systematically solving for varying orders of ε . We observe that as $\varepsilon \rightarrow 0$, the asymptotic expansion (15) reduces to

$$U_i = U_i^{(0)}, \quad i = 1, \dots, N+2, \quad (16)$$

which we refer to as the leading-order solution. Subsequently, substituting asymptotic approximations yields the dimensionally reduced closure of the SWME.

In this study, a viscous slip scaling is chosen such that the viscosity is $\nu = \mathcal{O}(\varepsilon^{-1})$, and the slip length is $\lambda = \mathcal{O}(\varepsilon^{-1})$. We introduce the following scalings, given by

$$\lambda = \frac{\lambda_0}{\varepsilon}, \quad \nu = \frac{\nu_0}{\varepsilon}, \quad (17)$$

where λ_0 and ν_0 are assumed dimensionless. The choice of a large slip length λ is motivated by the findings in [8], where the limit $\lambda \rightarrow \infty$ corresponds to a stable equilibrium with a constant velocity profile in the vertical direction and vanishing moment variables. In the vicinity of this equilibrium, where $\lambda \gg 1$ but remains finite, we investigate approximations of the moment variables α_j for $i = 1, \dots, N$. Moreover, we prove that by selecting a large viscosity $\nu = \mathcal{O}(\varepsilon^{-1})$, we can obtain a closure of the SWME model with dimensional reduction. In A, alternative scalings of friction parameters are discussed.

Applying the viscous slip scaling (17) to (7c) and letting $\varepsilon \rightarrow 0$ yields

$$\sum_{j=1}^N C_{ij} \alpha_j = 0, \quad \forall i = 1, \dots, N. \quad (18)$$

Equation (18) can be expressed in matrix-vector form as

$$\mathbf{C}_N \boldsymbol{\alpha}_N = \mathbf{0}, \quad (19)$$

where $\mathbf{C}_N \in \mathbb{R}^{N \times N}$ is a matrix with entries $C_{Nij} = C_{ij}$ and $\boldsymbol{\alpha}_N \in \mathbb{R}^N$ is a vector with entries $(\boldsymbol{\alpha}_N)_j = \alpha_j$, for $i, j = 1, \dots, N$. According to [8], the matrix \mathbf{C}_N is invertible. Therefore, the only possible leading order solution for (18) is $\alpha_j = 0, \forall j = 1, \dots, N$.

In [8], letting the slip variable $\lambda \rightarrow \infty$ results in a stable constant-velocity equilibrium in the HSWME and SWLME systems such that $\alpha_j = 0$ for $j = 1, \dots, N$. This large slip equilibrium corresponds to the viscous slip leading order solution from (19). In this study, our objective is to derive approximations for the viscous slip SWME system in the vicinity of $\alpha_j = 0$ for $j = 1, \dots, N$. Notably, setting the moment variables α_j ($j = 1, \dots, N$) to zero results in a hyperbolic system [12].

Under the scaling defined in (17), the equations governing h (7a) and hu_m (7b) do not depend on ε . Consequently, taking the limit $\varepsilon \rightarrow 0$ in the SWME does not yield a leading-order solution for either h or hu_m . Thus, this independence renders the derivation of asymptotic expansions for the variables h and u_m impossible. However, as demonstrated earlier, the equation for α_j , for $j = 1, \dots, N$, given by (7c), does admit a leading-order solution under the scaling (17). Subsequently, the variables α_i are asymptotically expanded as

$$\alpha_i = \alpha_i^{(0)} + \varepsilon \alpha_i^{(1)} + \varepsilon^2 \alpha_i^{(2)} + \mathcal{O}(\varepsilon^3), \quad i = 1, \dots, N. \quad (20)$$

These expansions (20) are then substituted into the governing system (7c).

In the remainder of this section, an order-of-magnitude analysis is performed, in which the terms of the leading order, first order, and second order in ε are systematically retained. This analysis enables a dimensional reduction of the system in the proximity of the viscous slip leading order solution, ensuring that the dynamics are captured at multiple scales of ε . The reduction process involves expressing the closure relations of α_j for $j = 1, \dots, N$ as functions of the remaining variables h and u_m , incorporating combinations of terms at varying orders of ε . Finally, substituting these asymptotic expansions as closure relations back into (7c) closes the system, yielding the Reduced Shallow Water Moment Equation (RSWME).

Note that these closure relations depend on the scaling. In A, we explore possible asymptotic approximations for the SWME using alternative scalings of the viscosity ν and slip length λ .

We begin by deriving closure relations and closed systems for the SWME (7a)-(7c) under the viscous slip scaling (17). The analysis proceeds systematically: in Subsection 3.1, we address the case $N = 1$; in Subsection 3.2, we extend the framework to $N = 2$; and in Subsection 3.3, we generalise the results to arbitrary N . A key finding is that for $N \geq 2$, all closed RSWME systems are identical.

Additionally, we analyse the hyperbolicity of these systems for $N = 1$, $N = 2$, and arbitrary N . Our analysis shows that none of these systems are globally hyperbolic. To resolve the loss of hyperbolicity, we introduce a hyperbolic regularisation.

3.1 Asymptotic expansion for SWME with $N = 1$

In [22], an asymptotic expansion for the coefficient α_1 is derived for the SWME from (7a)-(7c) with $N = 1$. We follow the explanation in [22], to present the main idea, before generalising to larger N . Let SWME1 denote the SWME model of order $N = 1$. When the viscous slip scaling from (17) is applied to SWME1, the governing equations become

$$\partial_t \begin{pmatrix} h \\ hu_m \\ h\alpha_1 \end{pmatrix} + \partial_x \begin{pmatrix} hu_m \\ hu_m^2 + \frac{1}{3}h\alpha_1^2 + g\frac{h^2}{2} \\ 2hu_m\alpha_1 \end{pmatrix} = \begin{pmatrix} 0 \\ 0 \\ u_m\partial_x(h\alpha_1) \end{pmatrix} - \frac{v_0}{\lambda_0} \begin{pmatrix} 0 \\ u_m + \alpha_1 \\ 3\left(u_m + \alpha_1 + \frac{4\lambda_0}{\varepsilon h}\alpha_1\right) \end{pmatrix}. \quad (21)$$

The last equation of (21) depends on ε , which motivates expanding the variable α_1 as

$$\alpha_1 = \alpha_1^{(0)} + \varepsilon\alpha_1^{(1)} + \varepsilon^2\alpha_1^{(2)} + \mathcal{O}(\varepsilon^3). \quad (22)$$

By substituting (22) into the last equation of system (21) and collecting terms of the same orders in ε , we obtain explicit expressions for the asymptotic components $\alpha_1^{(i)}$ ($i = 0, 1, 2$).

First, the $\mathcal{O}(\varepsilon^{-1})$ terms in the last equation of (21) are analysed to derive $\alpha_1^{(0)}$. Next, $\alpha_1^{(0)}$ is substituted back into the last equation of (21), and the $\mathcal{O}(\varepsilon^0)$ component is retained to determine the closure relation for $\alpha_1^{(1)}$. Finally, the $\mathcal{O}(\varepsilon^1)$ component of (21) is retained to derive the closure relation for $\alpha_1^{(2)}$.

The $\mathcal{O}(\varepsilon^{-1})$ -approximation of the SWME1 Let us substitute the asymptotic expansion (22) of α_1 into the last equation of (21). This substitution produces the $\mathcal{O}(\varepsilon^{-1})$ -order component of (21), which is given by

$$\frac{4\lambda_0}{h}\alpha_1^{(0)} = 0 \quad \Longrightarrow \quad \alpha_1^{(0)} = 0. \quad (23)$$

The $\mathcal{O}(\varepsilon^0)$ -approximation of the SWME1 By retaining the $\mathcal{O}(\varepsilon^0)$ -terms of the last evolution equation in system (21) and substituting $\alpha_1^{(0)} = 0$, the closure relation for $\alpha_1^{(1)}$ is obtained as

$$u_m + \frac{4\lambda_0}{h}\alpha_1^{(1)} = 0 \quad \Longrightarrow \quad \alpha_1^{(1)} = -\frac{u_m h}{4\lambda_0}. \quad (24)$$

The $\mathcal{O}(\varepsilon^1)$ -approximation of the SWME1 Substituting $\alpha_1^{(1)}$ from (24) into the $\mathcal{O}(\varepsilon)$ terms of (21) gives

$$\partial_t(h^2u_m) + 2\partial_x(h^2u_m^2) = u_m\partial_x(h^2u_m) - 3\frac{v_0}{\lambda_0}\left(u_m h - \frac{16\lambda_0^2}{h}\alpha_1^{(2)}\right). \quad (25)$$

To simplify (25), we use [22] to obtain

$$\partial_t(h^2u_m) = -\frac{1}{2}\partial_x(h^2u_m^2) - h\left[\partial_x\left(hu_m^2 + \frac{gh^2}{2}\right) + \frac{v_0}{\lambda_0}u_m\right]. \quad (26)$$

Equation (26) follows from applying the chain rule and combining the mass conservation equation and first equation of (21), with the $\mathcal{O}(\varepsilon^0)$ momentum terms in the second line of (21) [22].

Substituting (26) into (25), the closure relation for $\alpha_1^{(2)}$ is given by

$$\alpha_1^{(2)} = \frac{1}{48v_0\lambda_0}\left(-\frac{g}{4}\partial_x(h^4) + \frac{2v_0}{\lambda_0}u_m h^2\right). \quad (27)$$

The closed reduced SWME1 model Substituting (23), (24), and (25) into (22) the closure relation for α_1 is derived as

$$\alpha_1 = \varepsilon \left(-\frac{hu_m}{4\lambda_0} \right) + \varepsilon^2 \left[\frac{1}{48\nu_0\lambda_0} \left(-\frac{g}{4}\partial_x(h^4) + 2\frac{\nu_0 u_m h^2}{\lambda_0} \right) \right] + \mathcal{O}(\varepsilon^3). \quad (28)$$

To obtain a closed system for h and hu_m , substitute α_1 from (28) into (21). By neglecting terms of order $\mathcal{O}(\varepsilon^3)$ and higher, the closed Reduced Shallow Water Moment Equations for $N = 1$ (RSWME1) are defined as [22]

$$\begin{aligned} \partial_t h + \partial_x(hu_m) &= 0, \\ \partial_t(hu_m) + \partial_x \left(hu_m^2 T_1^1(h, u_m) + \frac{gh^2}{2} T_2^1(h, u_m) \right) &= -\frac{\nu_0 u_m}{\lambda_0} T_3^1(h, u_m), \end{aligned} \quad (29)$$

where

$$T_1^1(h, u_m) = 1 + \frac{\varepsilon^2 h^2}{48\lambda_0^2}, \quad T_2^1(h, u_m) = 1 - \frac{\varepsilon^2 h^2}{96\lambda_0^2}, \quad T_3^1(h, u_m) = 1 - \frac{\varepsilon h}{4\lambda_0} + \frac{\varepsilon^2 h^2}{24\lambda_0^2}. \quad (30)$$

Remark 1. The Boussinesq coefficient, which captures variations from a uniform velocity profile, is given by [15]

$$\beta = \frac{1}{hu_m^2} \int_{h_b}^{h_s} u(x, z, t)^2 dz. \quad (31)$$

In the context of the SWME1 framework in [9], this coefficient takes the form

$$\beta = 1 + \frac{1}{3} \frac{\alpha_1^2}{u_m^2}. \quad (32)$$

Substituting the closure relation (28) for α_1 and ignoring the terms $\mathcal{O}(\varepsilon^3)$ and $\mathcal{O}(\varepsilon^4)$ yields

$$\beta \approx 1 + \frac{1}{48} \frac{\varepsilon^2 h^2}{\lambda_0^2} = T_1^1(h, u_m). \quad (33)$$

This finding means that the advection term of the RSWME1 is consistent with the approximation of a vertical velocity profile using the Boussinesq coefficient. This fact highlights the relevance of our model in view of similar models in the literature, see [15].

We derived a closed system (29) for h and u_m that takes into account small deviations around the viscous slip leading order solution with a constant velocity profile using an explicit closure for α_1 of $\mathcal{O}(\varepsilon^2)$ that was computed using the order-of-magnitude approach for terms up to $\mathcal{O}(\varepsilon^2)$. This means that the RSWME1 system is in theory able to approximate the SWME1 with a large viscosity and a large slip length while only numerically solving a system for two variables instead of three.

The RSWME1 from (29) depend on the same variables as the SWE (1). Furthermore, as $\varepsilon \rightarrow 0$, the RSWME1 are consistent with the SWE. In contrast to the SWE, the friction term in the RSWME1 incorporates additional contributions proportional to $\varepsilon u_m h$ and $\varepsilon^2 u_m h^2$, which represent variations around the mean velocity u_m . Furthermore, the RSWME1 features additional $\mathcal{O}(\varepsilon^2)$ -linear combinations of $h^3 u_m^2$ and h^2 in the transport matrix on its left-hand side, which are not present in the SWE.

Hyperbolicity of the RSWME1 The RSWME1 system (29) can be expressed in non-conservative form as

$$\partial_t U + A^1(U) \partial_x U = S^1(U), \quad (34)$$

where $U = (h, hu_m)$, and the system matrix $A^1(U) \in \mathbb{R}^{2 \times 2}$ is given by

$$A^1(U) = \begin{pmatrix} 0 & 1 \\ -u_m^2 \left(1 - \frac{\varepsilon^2 h^2}{48\lambda_0^2} \right) + gh - \frac{g\varepsilon^2 h^3}{48\lambda_0^2} & 2u_m \left(1 + \frac{\varepsilon^2 h^2}{48\lambda_0^2} \right) \end{pmatrix}. \quad (35)$$

Additionally the source-term $S^1(U) \in \mathbb{R}^2$ is defined as

$$S^1(U) = \begin{pmatrix} 0 \\ -\frac{v_0 u_m}{\lambda_0} \left(1 - \frac{\varepsilon h}{4\lambda_0} + \frac{\varepsilon^2 h^2}{24\lambda_0^2} \right) \end{pmatrix} \quad (36)$$

The RSWME1 (in the form (34)) enable a deeper analysis of the system. The eigenvalues of the matrix $A^1(U)$ from (35) correspond to the propagation speeds of the waves, a critical property of the system. If these eigenvalues are complex, real propagation speeds no longer exist, potentially leading to instabilities. In this subsection, we investigate whether hyperbolicity is preserved in (34).

To analyse hyperbolicity, we determine whether the eigenvalues $\lambda_{1,2}$ of $A^1(U)$ from (35) are real and distinct. These eigenvalues are given by

$$\lambda_{1,2} = u_m \left(1 + \frac{h^2 \varepsilon^2}{48\lambda_0^2} \right) \pm \sqrt{gh} \sqrt{\frac{\varepsilon^4 h^3 u_m^2}{2304\lambda_0^4 g} - \frac{\varepsilon^2 h^2}{48\lambda_0^2} + \frac{\varepsilon^2 h u_m^2}{16\lambda_0^2 g} + 1}. \quad (37)$$

For hyperbolicity, a positive discriminant is required, which is

$$\left(\frac{\varepsilon^4 h^3}{2304\lambda_0^4 g} + \frac{\varepsilon^2 h}{16\lambda_0^2 g} \right) u_m^2 - \frac{\varepsilon^2 h^2}{48\lambda_0^2} + 1 \geq 0. \quad (38)$$

Given the difficulty of determining h and u_m for which Condition (38) holds, we first analyse the case where $u_m = 0$. For hyperbolicity in this specific case, the following condition on h must hold

$$0 < h < \frac{4\sqrt{3}\lambda_0}{\varepsilon}. \quad (39)$$

Because the terms in (38) depending on u_m^2 increase monotonically with u_m , hyperbolicity at $u_m = 0$ means that hyperbolicity holds for all $u_m > 0$.

Condition (39) imposes that $\frac{h}{\lambda} = \frac{h\varepsilon}{\lambda_0} = \mathcal{O}(\varepsilon)$ must remain below a threshold, in line with the scaling ($\varepsilon \ll 1$). Consequently, hyperbolicity breaks down when the RSWME1 no longer capture the viscous slip regime.

Theorem 1 (Hyperbolic regularisation of RSWME1). *The RSWME1 system (29) admits a globally hyperbolic regularisation by adding the following term to the left-hand side of its last equation:*

$$\partial_x \left(\frac{4\varepsilon^4 h^6 g}{6 \cdot 192^2 \lambda_0^4} \right), \quad (40)$$

Proof. To establish global hyperbolicity, we augment the last equation of system (29) with the regularisation term (40), such that the modified system matrix (35) is given by

$$A^{1,H} = \begin{pmatrix} 0 & 1 \\ -u_m^2 \left(1 - \frac{\varepsilon^2 h^2}{48\lambda_0^2} \right) + gh - \frac{\varepsilon^2 h^3 g}{48\lambda_0^2} + \frac{4h^5 \varepsilon^4 g}{192^2 \lambda_0^4} & 2u_m \left(1 + \frac{\varepsilon^2 h^2}{48\lambda_0^2} \right) \end{pmatrix}. \quad (41)$$

The eigenvalues of the system matrix (41) of the Hyperbolic RSWME1 (HRSWME1) are

$$\lambda_{1,2} = u_m \left(1 + \frac{h^2 \varepsilon^2}{48\lambda_0^2} \right) \pm \sqrt{gh} \sqrt{\frac{\varepsilon^4 h^3 u_m^2}{2304\lambda_0^4 g} - \frac{\varepsilon^2 h^2}{48\lambda_0^2} + \frac{\varepsilon^2 h u_m^2}{16\lambda_0^2 g} + 1 + \frac{4\varepsilon^4 h^4}{192^2 \lambda_0^4}}. \quad (42)$$

For the special case where $u_m = 0$, the eigenvalues are

$$\lambda_{1,2} = \pm \sqrt{gh} \left(1 - \frac{2h^2}{192\lambda_0^2} \varepsilon^2 \right). \quad (43)$$

The term under the square root in (42) is strictly positive for all $h > 0$ when $u_m = 0$, and hence this value remains positive for all u_m as the terms containing u_m are greater or equal than zero for $h > 0$. Thus, for all $h > 0$ and u_m , the eigenvalues of (41) are real and distinct, ensuring the global hyperbolicity of HRSWME1. \square

It is important to note that the inclusion of the $\mathcal{O}(\varepsilon^4)$ -term (40) does not reduce the accuracy of the HRSWME1, given that the RSWME1 are of order $\mathcal{O}(\varepsilon^2)$.

3.2 Asymptotic expansion for SWME with $N = 2$

In this subsection, the $\mathcal{O}(\varepsilon^2)$ -order SWME for $N = 2$ (SWME2) are simplified using asymptotic approximations, in preparation for deriving a reduced SWME system for arbitrary N . This reduction decreases the system from four to two equations, analogous to the previously derived $N = 1$ case. The viscous slip system SWME2 based on (7a)-(7c) are given by

$$\partial_t \begin{pmatrix} h \\ hu_m \\ h\alpha_1 \\ h\alpha_2 \end{pmatrix} + \partial_x \begin{pmatrix} hu_m \\ hu_m^2 + \frac{1}{3}h\alpha_1^2 + \frac{1}{5}h\alpha_2^2 + g\frac{h^2}{2} \\ 2hu_m\alpha_1 + \frac{4}{5}\alpha_1\alpha_2 \\ 2hu_m\alpha_2 + \frac{2}{3}h\alpha_1^2 + \frac{2}{7}h\alpha_2^2 \end{pmatrix} = \begin{pmatrix} 0 \\ 0 \\ (u_m - \frac{1}{5}\alpha_2)\partial_x(h\alpha_1) + \frac{1}{5}\alpha_1\partial_x(h\alpha_2) \\ \alpha_1\partial(h\alpha_1) + (u_m + \frac{\alpha_2}{7})\partial_x(h\alpha_2) \end{pmatrix} \quad (44)$$

$$- \frac{v_0}{\lambda_0} \begin{pmatrix} 0 \\ u_m + \alpha_1 + \alpha_2 \\ 3(u_m + \alpha_1 + \alpha_2 + \frac{4\lambda_0}{\varepsilon h}\alpha_1) \\ 5(u_m + \alpha_1 + \alpha_2 + \frac{12\lambda_0}{\varepsilon h}\alpha_2) \end{pmatrix}.$$

Similar to the RSWME1 case in Subsection 3.1, the asymptotic expansions for α_1 and α_2 are expressed as

$$\alpha_1 = \alpha_1^{(0)} + \varepsilon\alpha_1^{(1)} + \varepsilon^2\alpha_1^{(2)} + \mathcal{O}(\varepsilon^3), \quad (45)$$

$$\alpha_2 = \alpha_2^{(0)} + \varepsilon\alpha_2^{(1)} + \varepsilon^2\alpha_2^{(2)} + \mathcal{O}(\varepsilon^3). \quad (46)$$

By substituting (45) and (46) into the final two equations of system (44), the coefficients $\alpha_i^{(i)}$ and $\alpha_2^{(i)}$ for $i = 0, 1, 2$ are systematically derived order by order.

The $\mathcal{O}(\varepsilon^{-1})$ approximation of the SWME2 Substitute the asymptotic expansions (45) and (46) into the final two equations of (44) and retain only the $\mathcal{O}(\varepsilon^{-1})$ -order terms. Solving for $\alpha_1^{(0)}$ and $\alpha_2^{(0)}$ yields

$$\begin{pmatrix} \alpha_1^{(0)} \\ \alpha_2^{(0)} \end{pmatrix} = \mathbf{0}. \quad (47)$$

The $\mathcal{O}(\varepsilon^0)$ approximation of the SWME2 Retaining only the $\mathcal{O}(\varepsilon^0)$ -order terms in (44) and incorporating (47), we solve for $\alpha_1^{(1)}$ and $\alpha_2^{(1)}$ to obtain

$$\begin{pmatrix} \alpha_1^{(1)} \\ \alpha_2^{(1)} \end{pmatrix} = \begin{pmatrix} -\frac{hu_m}{4\lambda_0} \\ -\frac{hu_m}{12\lambda_0} \end{pmatrix}. \quad (48)$$

The $\mathcal{O}(\varepsilon^1)$ approximation of the SWME2 The $\mathcal{O}(\varepsilon)$ -order contribution of (44) yields closure relations

$$\begin{pmatrix} \alpha_1^{(2)} \\ \alpha_2^{(2)} \end{pmatrix} = \frac{1}{v_0\lambda_0} \begin{pmatrix} \frac{1}{48} \left(-\frac{g}{4}\partial_x(h^4) + 3\frac{v_0u_m h^2}{\lambda_0} \right) \\ \frac{1}{720} \left(-\frac{g}{4}\partial_x(h^4) + 19\frac{v_0u_m h^2}{\lambda_0} \right) \end{pmatrix}. \quad (49)$$

The closure relations from (49) follow the derivation steps of $\alpha_1^{(2)}$ in Subsection 3.1.

The closed reduced SWME2 model Substituting the closure relations from (47), (48), and (49) into the asymptotic expansions (45)-(46) leads to the closure relations for the coefficients α_1 and α_2 :

$$\alpha_1 = \varepsilon \left(-\frac{hu_m}{4\lambda_0} \right) + \varepsilon^2 \left(\frac{1}{48v_0\lambda_0} \left(-\frac{g}{4}\partial_x(h^4) + 3\frac{v_0u_m h^2}{\lambda_0} \right) \right) + \mathcal{O}(\varepsilon^3), \quad (50)$$

$$\alpha_2 = \varepsilon \left(-\frac{hu_m}{12\lambda_0} \right) + \varepsilon^2 \left(\frac{1}{720v_0\lambda_0} \left(-\frac{g}{4}\partial_x(h^4) + 19\frac{v_0u_m h^2}{\lambda_0} \right) \right) + \mathcal{O}(\varepsilon^3). \quad (51)$$

To obtain the closed system for h and hu_m , the expressions for α_1 and α_2 from (50) and (51) are substituted into the second and third equations of (44). As we neglect higher order terms of order $\mathcal{O}(\varepsilon^3)$ and higher, the closed Reduced SWME2 (RSWME2) are given by

$$\begin{aligned}\partial_t h + \partial_x(hu_m) &= 0, \\ \partial_t(hu_m) + \partial_x\left(hu_m^2 T_1^2(h, u_m) + \frac{gh^2}{2} T_2^2(h, u_m)\right) &= -\frac{v_0 u_m}{\lambda_0} T_3^2(h, u_m),\end{aligned}\tag{52}$$

where

$$T_1^2(h, u_m) = 1 + \frac{\varepsilon^2 h^2}{45\lambda_0^2}, \quad T_2^2(h, u_m) = 1 - \frac{\varepsilon^2 h^2}{90\lambda_0^2}, \quad T_3^2(h, u_m) = 1 - \frac{\varepsilon h}{3\lambda_0} + \frac{\varepsilon^2 h^2}{45\lambda_0^2}.$$

Observe that the RSWME2 in (52) share the same structure as the RSWME1 from (29). The only difference arises from the constants that scale the $\mathcal{O}(\varepsilon)$ and $\mathcal{O}(\varepsilon^2)$ terms.

Observe that one can derive the Boussinesq coefficient for the RSWME2, as in Remark 1. Repeating this procedure will show that the RSWME2 system also has an advection term consistent with the Boussinesq-coefficient-based approximation of the vertical velocity profile.

Hyperbolicity of the RSWME2 The system in (52) can be expressed in non-conservative form as

$$\partial_t U + A^2(U) \partial_x U = S^2(U),\tag{53}$$

where $U = (h, hu_m)$. The system matrix $A^2(U) \in \mathbb{R}^{2 \times 2}$ is given by

$$A^2(U) = \begin{pmatrix} 0 & 1 \\ -u_m^2 \left(1 - \frac{\varepsilon^2 h^2}{45\lambda_0^2}\right) + gh - \frac{g\varepsilon^2 h^3}{45\lambda_0^2} & 2u_m \left(1 + \frac{\varepsilon^2 h^2}{45\lambda_0^2}\right) \end{pmatrix}.\tag{54}$$

Additionally, the source term is given by $S^2(U) \in \mathbb{R}^2$ as

$$S^2(U) = \begin{pmatrix} 0 \\ -\frac{v_0 u_m}{\lambda_0} \left(1 - \frac{\varepsilon h}{3\lambda_0} + \frac{\varepsilon^2 h^2}{45\lambda_0^2}\right) \end{pmatrix}\tag{55}$$

To analyse hyperbolicity, we determine whether the eigenvalues $\lambda_{1,2}$ of $A^2(U)$ from (54) are real and distinct. These eigenvalues are given by

$$\lambda_{1,2} = u_m \left(1 + \frac{h^2 \varepsilon^2}{45\lambda_0^2}\right) \pm \sqrt{gh} \sqrt{\frac{\varepsilon^4 h^3 u_m^2}{2025\lambda_0^4 g} - \frac{\varepsilon^2 h^2}{45\lambda_0^2} + \frac{\varepsilon^2 h u_m^2}{15\lambda_0^2 g} + 1}.\tag{56}$$

For hyperbolicity, the condition that must be satisfied is

$$\left(\frac{\varepsilon^4 h^3}{2025\lambda_0^4 g} + \frac{\varepsilon^2 h}{15\lambda_0^2 g}\right) u_m^2 - \frac{\varepsilon^2 h^2}{45\lambda_0^2} + 1 \geq 0.\tag{57}$$

Similar to analysing the hyperbolicity of the RSWME1 system, we begin by analysing the hyperbolicity for $u_m = 0$. For this specific case, hyperbolicity requires that the following condition on h is satisfied

$$0 < h < \frac{3\sqrt{5}\lambda_0}{\varepsilon}.\tag{58}$$

The terms depending on u_m on the left-hand side of Equation (57) are always positive for $h > 0$ and any non-zero value of u_m . Satisfying Condition (58) in the case where $u_m = 0$, ensures that hyperbolicity holds for all $u_m \geq 0$.

Condition (58) imposes that $\frac{h}{\lambda} = \frac{h\varepsilon}{\lambda_0} = \mathcal{O}(\varepsilon)$ must remain below a threshold, in line with the scaling ($\varepsilon \ll 1$). Consequently, hyperbolicity breaks down when the RSWME2 no longer capture the viscous slip regime.

Theorem 2 (Hyperbolic regularisation of RSWME2). *The RSWME2 system, as defined in Equation (52), admits a globally hyperbolic regularisation through the addition of the following term to the left-hand side of its last equation:*

$$\partial_x \left(\frac{4\varepsilon^4 h^6 g}{6 \cdot 180^2 \lambda_0^4} \right). \quad (59)$$

Proof. This result follows analogously to the proof of Theorem 1. \square

3.3 Asymptotic expansion for SWME with arbitrary N

This section presents the derivation of solutions for an arbitrary number of moments, denoted by N . The order analysis for arbitrary N employs asymptotic expansions of the form

$$\alpha_{N,i} = \alpha_{N,i}^{(0)} + \varepsilon \alpha_{N,i}^{(1)} + \varepsilon^2 \alpha_{N,i}^{(2)} + \mathcal{O}(\varepsilon^3), \quad i = 1, \dots, N, \quad (60)$$

and will be substituted in (7a)–(7c). Note that we use the notation $\alpha_{N,i}$, for $i = 1, \dots, N$ to denote the moment variable α_i in a SWME of order N . In the remainder of this subsection we derive the closure relations for $\alpha_{N,i}$, which may also vary depending on N .

The $\mathcal{O}(\varepsilon^{-1})$ approximation of the SWME Substitution of the asymptotic expansions (60) for $i = 1, \dots, N$ into Equation (7c) yields the $\mathcal{O}(\varepsilon^{-1})$ -order term

$$\frac{v_0}{h} \left(\sum_{j=1}^N C_{ij} \alpha_{N,j}^{(0)} \right) = 0. \quad (61)$$

The system (61) in matrix-vector form is

$$\mathbf{C}_N \boldsymbol{\alpha}_N^{(0)} = \mathbf{0}, \quad (62)$$

where $\mathbf{C}_N \in \mathbb{R}^{N \times N}$ is as defined in (19) and $\boldsymbol{\alpha}_N^{(0)}$ is the vector whose j -th component corresponds to $\alpha_{N,j}^{(0)}$. As shown in [8], the matrix \mathbf{C}_N is invertible, and as a result the solution is

$$\alpha_{N,i}^{(0)} = 0, \quad i = 1, \dots, N. \quad (63)$$

The $\mathcal{O}(\varepsilon^0)$ approximation of the SWME Substituting (63) into the $\mathcal{O}(\varepsilon^0)$ -order system (7c) yields N closure relations for the coefficient variable $\alpha_{N,j}^{(1)}$:

$$\sum_{j=1}^N C_{ij} \alpha_{N,j}^{(1)} = -\frac{u_m h}{\lambda_0},$$

where $i = 1, \dots, N$. In matrix-vector form, the solution for $\boldsymbol{\alpha}_N^{(1)} \in \mathbb{R}^N$ can be expressed as

$$\mathbf{C}_N \boldsymbol{\alpha}_N^{(1)} = -\mathbf{1} \frac{u_m h}{\lambda_0}, \quad (64)$$

where $\mathbf{C}_N \in \mathbb{R}^{N \times N}$ has entries $C_{Nij} = C_{ij}$, $\boldsymbol{\alpha}_N^{(1)}$ is the vector of first-order coefficients with the following entries $(\boldsymbol{\alpha}_N^{(1)})_i = \alpha_{N,i}^{(1)}$ (for $i = 1, \dots, N$) and $\mathbf{1} \in \mathbb{R}^N$ is the vector of ones. Rewriting Equation (64) yields closure relations for the coefficients $\alpha_{N,i}^{(1)}$ ($i = 1, \dots, N$):

$$\alpha_{N,i}^{(1)} = -\frac{u_m h}{\lambda_0} \sum_{j=1}^N (\mathbf{C}_N^{-1})_{ij}. \quad (65)$$

Thus, the closure relation $\alpha_{N,i}^{(1)}$, for $i = 1, \dots, N$ can be expressed as

$$\alpha_{N,i}^{(1)} = -\frac{1}{\lambda_0} \tilde{B}_i^{(N)} u_m h, \quad (66)$$

where $\tilde{B}_i^{(N)} \in \mathbb{R}$ is a constant independent of u_m, h, t , and x , and is given by

$$\tilde{B}_i^{(N)} = \sum_{j=1}^N (C_N^{-1})_{ij}. \quad (67)$$

The $\mathcal{O}(\varepsilon^1)$ approximation of the SWME We substitute the solutions from (63) and (65) into the $\mathcal{O}(\varepsilon)$ -order terms of Equation (7c). Solving for $\alpha_{i,N}^{(2)}$ ($i = 1, \dots, N$) yields the following closure relations for $\alpha_N^{(2)} \in \mathbb{R}^N$

$$\tilde{C}_N \alpha_N^{(2)} = -\frac{g}{4v_0 \lambda_0} (\tilde{I}_1^N \mathbf{1}) \partial_x (h^4) - \frac{1}{\lambda_0^2} (\tilde{I}_2^N \mathbf{1}) u_m h^2, \quad (68)$$

where $\tilde{C}_N \in \mathbb{R}^{N \times N}$, $\tilde{I}_1^N \in \mathbb{R}^{N \times N}$ and $\tilde{I}_2^N \in \mathbb{R}^{N \times N}$ are matrices with the entries for $i, j = 1, \dots, N$ given by

$$\tilde{C}_{Nij} = (2i+1)C_{ij}, \quad (69)$$

$$(\tilde{I}_1^N)_{ij} = (C_N^{-1})_{ij}, \quad (70)$$

$$(\tilde{I}_2^N)_{ij} = (C_N^{-1})_{ij} - (2i+1) \left(\sum_{k,l=1}^N (C_N^{-1})_{kl} \right) \delta_{ij}. \quad (71)$$

For $i = 1, \dots, N$, rewrite Equation (68) as

$$\alpha_{N,i}^{(2)} = \frac{1}{\lambda_0^2} \tilde{D}_i^{(N)} u_m h^2 - \frac{g}{4v_0 \lambda_0} \tilde{F}_i^{(N)} \partial_x (h^4), \quad (72)$$

where $\tilde{D}_i^{(N)}$ and $\tilde{F}_i^{(N)} \in \mathbb{R}$ are constants independent of u_m, h, x , and t . The explicit expressions for $\tilde{D}_i^{(N)}$ and $\tilde{F}_i^{(N)}$ are

$$\tilde{D}_i^{(N)} = -\sum_{j=1}^N (\tilde{C}_N^{-1} C_N^{-1})_{ij} + \left(\sum_{k,l=1}^N (C_N^{-1})_{k,l} \right) \left(\sum_{j=1}^N (C_N^{-1})_{ij} \right), \quad (73)$$

$$\tilde{F}_i^{(N)} = \sum_{j=1}^N (\tilde{C}_N^{-1} C_N^{-1})_{ij}. \quad (74)$$

The closed RSWME model for arbitrary N Substituting (63), (66) and (72) into (60), we obtain the closure relation for $\alpha_{N,j}$ ($j = 1, \dots, N$) as

$$\alpha_{N,j} = -\frac{\varepsilon}{\lambda_0} \tilde{B}_j^{(N)} u_m h + \varepsilon^2 \left(\frac{1}{\lambda_0^2} \tilde{D}_j^{(N)} u_m h^2 - \frac{g}{4v_0 \lambda_0} \tilde{F}_j^{(N)} \partial_x (h^4) \right) + \mathcal{O}(\varepsilon^3). \quad (75)$$

Substituting (75) into (7b) and ignoring the terms $\mathcal{O}(\varepsilon^3)$ and $\mathcal{O}(\varepsilon^4)$ produces a closed RSWME system that takes the following form

$$\partial_t U + A^N(U) \partial_x U = S^N(U). \quad (76)$$

The system matrix $A^N(U) \in \mathbb{R}^{2 \times 2}$ of (76) is defined as

$$A^N = \begin{pmatrix} 0 & 1 \\ -u_m^2 \left(1 - \frac{\varepsilon^2 h^2}{\lambda_0^2} \Gamma^N \right) + gh \left(1 - \frac{\varepsilon^2 h^2}{\lambda_0 v_0} \Phi^N \right) & 2u_m \left(1 + \frac{\varepsilon^2 h^2}{\lambda_0^2} \Gamma^N \right) \end{pmatrix}, \quad (77)$$

where the constants Γ^N and $\Phi^N \in \mathbb{R}$ are given by

$$\Gamma^N = \sum_{j=1}^N \frac{(\tilde{B}_j^{(N)})^2}{2j+1}, \quad \Phi^N = \sum_{j=1}^N \tilde{F}_j^{(N)}. \quad (78)$$

The source term $S^N(U) \in \mathbb{R}^2$ in (76) is

$$S^N(U) = \begin{pmatrix} 0 \\ -\frac{v_0}{\lambda_0} u_m \left(1 - \frac{\varepsilon}{\lambda_0} \Omega^N h + \frac{\varepsilon^2}{\lambda_0^2} \Lambda^N h^2 \right) \end{pmatrix}, \quad (79)$$

where the constants Ω^N and $\Lambda^N \in \mathbb{R}$ are defined as

$$\Omega^N = \sum_{i=1}^N \tilde{B}_i^{(N)}, \quad \Lambda^N = \sum_{i=1}^N \tilde{D}_i^{(N)}. \quad (80)$$

We further present the following theorem regarding the RSWME of order N .

Theorem 3 (Identical closed RSWME systems). *For $N \geq 2$, all RSWME systems are identical.*

Proof. The detailed proof is provided in B. □

From Theorem 3 we know that for all $N \geq 2$ the system matrix $A^N \in \mathbb{R}^{2 \times 2}$ from (77) and the source term $S^N \in \mathbb{R}^2$ from (79) remain unchanged. As a result, using the numerically computed values of h and u_m from the RSWME2 system, the velocity profile (3) can be obtained for arbitrary N by substituting these solutions into the closure relations for $\alpha_{N,i}$, for $i = 1, \dots, N$ from (72) in a post processing step.

In theory, the RSWME achieve a substantial reduction in runtime relative to the SWME, which uses a much larger system of equations, scaling with dimension $N + 2$.

Hyperbolicity of the RSWME for arbitrary N As a consequence of Theorem 3, the hyperbolicity conditions for arbitrary $N \geq 2$ are identical to those for the case $N = 2$, as specified by condition (58). For arbitrary N , the model is hyperbolic, provided that the assumptions $\lambda = \mathcal{O}(\varepsilon^{-1})$ and $\nu = \mathcal{O}(\varepsilon^{-1})$ are satisfied, where $\varepsilon \ll 1$ is a small scaling. Moreover, the hyperbolic regularisation approach for $N = 2$, as presented in Theorem 2, can be extended to ensure global hyperbolicity for arbitrary N . Hence, for arbitrary $N \geq 2$, global hyperbolicity could be obtained by adding the regularisation term from (59) to the left-hand side of (76).

4 Numerical simulation

In this section, we first present the time-integration scheme needed to handle the stiff source term for the viscous slip SWME. We then present three numerical tests: a wave with sharp gradients (based on [12]), a smooth sine wave, and an initial square root velocity profile.

To examine the accuracy and computational cost of the RSWME and its closure relations for the moment variables, we conduct numerical experiments, where the SWME are used as a reference solution.

4.1 Numerical methods

For large scalings of slip length λ and viscosity ν as given by (17), the source term $S(U)$ in the SWME system (14) is of order $\mathcal{O}(\varepsilon^{-1})$. This scaling can introduce stiffness, potentially leading to numerical instabilities. To avoid these numerical instabilities, operator splitting is employed in [8], allowing the source term to be integrated implicitly while maintaining stability in the numerical scheme.

In [8], the SWME model (7a)-(7c) is split into two parts as follows

$$\partial_t U + A(U) \partial_x U = 0, \quad (81)$$

$$\partial_t U = S(U). \quad (82)$$

Table 1: Numerical setup for wave with sharp gradient simulation.

viscosity	$\nu \in \{100, 10, 1\}$
slip length	$\lambda \in \{100, 10, 1\}$
temporal domain	$t \in [0, 2]$
spatial domain	periodic $x \in [-1, 1]$
spatial resolution	$n_x = 1000$
initial height	$h(x, 0) = 1 + \exp(3 \cos(\pi(x + 0.5))) - 4.0$
initial velocity profile	$u(x, 0, \xi) = 0.5\xi$
CFL condition	0.7
numerical scheme	PRICE [4, 5]

To solve (81), we use a path-conservative finite volume scheme based on the polynomial viscosity methods developed for non-conservative products described in [4, 5], with linear paths and polynomial viscosity matrix. For the source term in (82), an implicit backward Euler scheme is employed, resulting in

$$\frac{U^{n+1} - U^n}{\Delta t} = S(U^{n+1}), \quad (83)$$

where U^n denotes the vector U evaluated at the discrete time $t = t^n$, such that t^n corresponds to the n -th time step. Because S is linear, the system (83) can be solved directly by inverting a matrix, similar to [8].

Under the assumption that $\lambda = \mathcal{O}(\varepsilon^{-1})$ and $\nu = \mathcal{O}(\varepsilon^{-1})$, the source terms corresponding to SWE (1) and the RSWME (76) are of order $\mathcal{O}(1)$. Consequently, these source terms do not exhibit stiffness, thereby permitting the choice of an explicit numerical scheme for the source term. In this work, the explicit scheme to solve (82) within the SWE and RSWME model is given by

$$\frac{U^{n+1} - U^n}{\Delta t} = S(U^n). \quad (84)$$

4.2 Test I wave with a sharp height gradient

To assess the accuracy of the RSWME1 model, we conduct a wave test with a sharp height gradient and compare the results with those obtained from the SWME1 model. The configuration of this test is provided in Table 1.

For this analysis, we adopt the wave test from [12], while modifying only the values of the viscosity ν and slip length λ such that (17) holds. We evaluate the numerical results of the RSWME model for various values of $\varepsilon \in \{0.01, 0.1, 1\}$. The smallest value, $\varepsilon = 0.01$, aligns with the equilibrium assumptions where $\varepsilon \ll 1$. The intermediate value, $\varepsilon = 0.1$, corresponds to a moderate deviation from equilibrium, while the largest value, $\varepsilon = 1$, represents a significant shift away from equilibrium, invalidating the assumption that $\varepsilon \ll 1$.

In Equation (17), we set $\lambda_0 = 1$ and $\nu_0 = 1$. Consequently, in our simulations, we use $\lambda = \nu = \varepsilon^{-1}$.

For the spatial discretisation, we employ a PRICE scheme within the framework of polynomial viscosity methods [4, 5].

Numerical experiments were conducted for the various values of ε over a time span of two seconds. In Figure 1, the numerical solutions for the average velocity u_m and height h from the SWE, RSWME1, and SWME1 systems are presented. For $\varepsilon = 0.01$ and $\varepsilon = 0.1$, the SWE, RSWME1, and SWME1 solutions are indistinguishable. In the limit as $\varepsilon \rightarrow 0$, the RSWME1 align with the SWE. According to [8], $\lambda \rightarrow \infty$ represents an equilibrium where the moment coefficients vanish. Since $\lambda \rightarrow \infty$ as $\varepsilon \rightarrow 0$, the moment variables in the SWME1 model become negligible for small ε .

For $\varepsilon = 1$, there are significant differences between the models. In particular, The RSWME1 provide a closer approximation to the average velocity u_m of the SWME1 than the SWE do.

The relative L_1 -errors for the SWE and RSWME1 models, computed using SWME1 as the reference, are

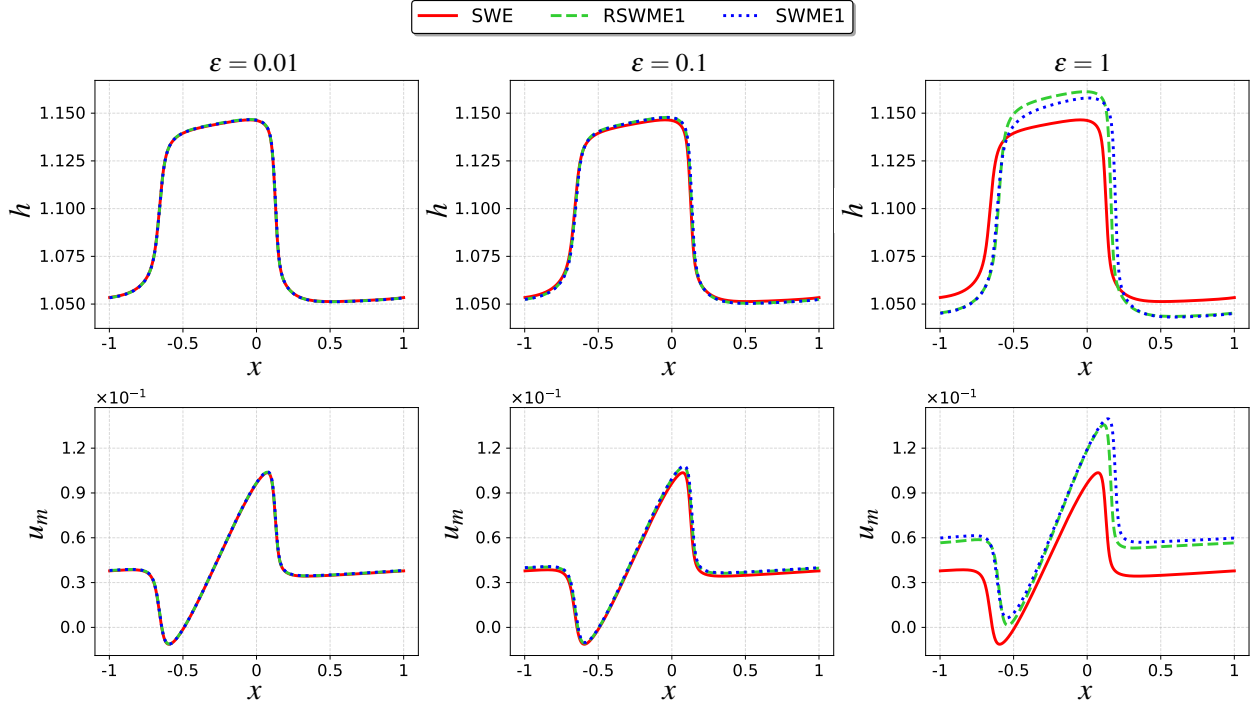


Figure 1: Wave with a sharp gradient test comparing the SWE (red, solid), RSWME1 (green, dashed), and SWME1 (blue, dotted) models at $t = 2.0$. The results are presented for the height h (top row) and velocity u_m (bottom row) across three values of ϵ : $\epsilon = 0.01$ (left), $\epsilon = 0.1$ (middle), and $\epsilon = 1$ (right).

given by

$$\begin{aligned}
 E_{\text{SWE},h} &= \frac{\|h_{\text{SWE}} - h_{\text{SWME}}\|_1}{\|h_{\text{SWME}}\|_1}, & E_{\text{SWE},u_m} &= \frac{\|u_{m,\text{SWE}} - u_{m,\text{SWME}}\|_1}{\|u_{m,\text{SWME}}\|_1}, \\
 E_{\text{RSWME},h} &= \frac{\|h_{\text{RSWME}} - h_{\text{SWME}}\|_1}{\|h_{\text{SWME}}\|_1}, & E_{\text{RSWME},u_m} &= \frac{\|u_{m,\text{RSWME}} - u_{m,\text{SWME}}\|_1}{\|u_{m,\text{SWME}}\|_1}.
 \end{aligned}$$

In Table 2, the RSWME1 yield a solution for height h and average velocity u_m that better approximates the SWME1 compared to the SWE for $\epsilon \in \{0.01, 0.1, 1\}$.

By substituting the numerically computed solutions for h and u_m into the closure relation (28), we compute the coefficient α_1 . The closure relation in (28) involves the spatial derivative of h^4 with respect to x , which we approximate numerically using a Godunov scheme. Experiments with various FVM schemes to discretise $\partial_x(h^4)$ revealed no significant differences. Thus, comparative analyses are omitted for conciseness.

In Figure (2), the numerical solution for α_1 from the SWME1 model, as well as the approximated solution for α_1 via the closure relation (28), are shown. One can observe that for $\epsilon = 0.01$, both solutions converge to zero. For $\epsilon = 0.1$, both the SWME1 and RSWME1 solutions equally deviate from zero, which indicates high accuracy of the RSWME1 model. However, for $\epsilon = 1$, large peaks occur in the approximated solution via the RSWME1 solution. This can be explained as follows, the closure relation in (28) includes a term of the form $-\epsilon^2 \frac{\partial_x(h^4)}{4g}$. When $\epsilon = 1$ and the solution features sharp gradients in h , this term can lead to significant peaks in the resulting solution for α_1 . To investigate these deviations, as observed in Figure 2, we examine the numerical derivative of h^4 with respect to x for the SWE, RSWME, and SWME models. Figure 3 displays this derivative across different values of ϵ . For $\epsilon = 1$, both the SWME and RSWME yield significantly larger values of $\partial_x(h^4)$ compared to the SWE. Because this derivative is further scaled by ϵ^2 , the resulting peaks are not damped as in the case $\epsilon \ll 1$. To observe for which cases these peaks do not occur in the reconstruction of the moments, we present a smooth case with a smaller gradient of h in the next subsection.

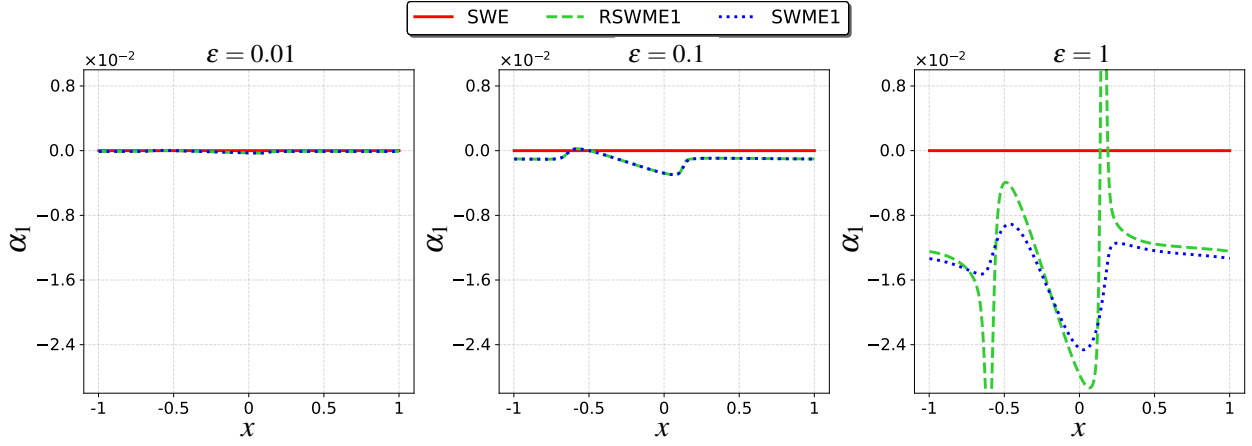


Figure 2: Wave with a sharp gradient test comparing the SWE (red, solid), RSWME1 (green, dashed), and SWME1 (blue, dotted) models at $t = 2.0$. The results are presented for the moment coefficient α_1 across three values of ε : $\varepsilon = 0.01$ (left), $\varepsilon = 0.1$ (middle), and $\varepsilon = 1$ (right).

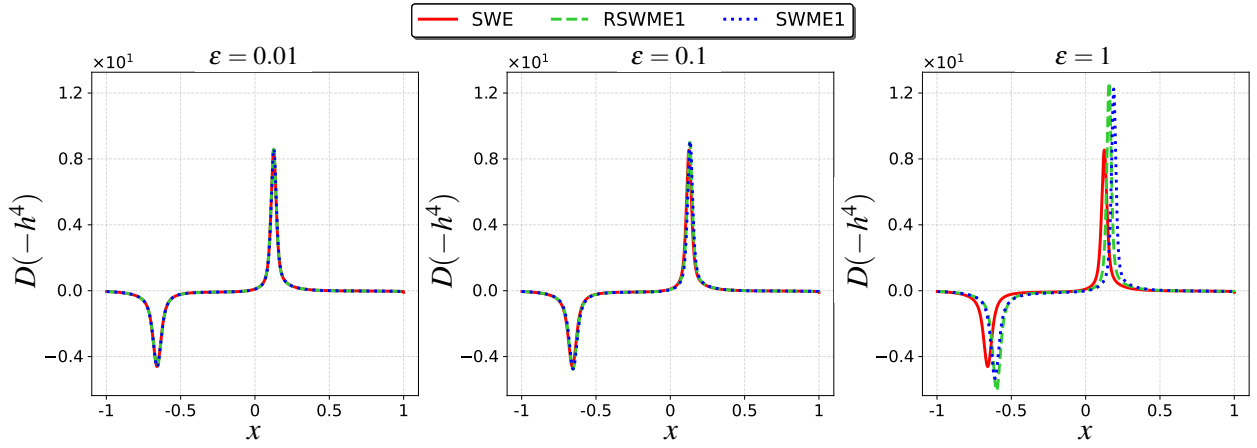


Figure 3: Wave with a sharp gradient test comparing the SWE (red, solid), RSWME1 (green, dashed), and SWME1 (blue, dotted) models at $t = 2.0$. The post processed $\partial_x(h^4)$ -value computed with Godunov reconstruction is shown across three values of ε : $\varepsilon = 0.01$ (left), $\varepsilon = 0.1$ (middle), and $\varepsilon = 1$ (right).

Table 2: Relative L_1 -error ($t = 2.0$, $N = 1$) for the wave with a sharp gradient.

	$\varepsilon = 0.01$	$\varepsilon = 0.1$	$\varepsilon = 1$
SWE, in h	1.4600e-04	1.2321e-03	1.0933e-02
RSWME1, in h	1.1144e-04	2.5440e-04	2.9279e-03
SWE, in u	7.3797e-03	5.6935e-02	3.7623e-01
RSWME1, in u	2.7112e-03	1.0151e-02	6.4229e-02

4.3 Test II: smooth sine wave

To investigate whether selecting an initial condition with smoother gradients leads to more accurate moment solutions via the closure relations, we present a smooth sine wave test case in Table 3.

Numerical tests for the smooth sine wave cases were conducted for the same values of ε over a duration of two seconds. The simulations focussed on the case where $N = 1$, employing the SWE, RSWME1, and SWME1. In Figure 4, the numerical solutions for the average velocity u_m and height h are presented. For $\varepsilon = 0.01$ and $\varepsilon = 0.1$, the SWE, RSWME1, and SWME1 solutions for height h are very similar. For $\varepsilon = 1$, the RSWME1 yield a numerical solution that is closer to the SWME1 compared to the SWE for both height

Table 3: Numerical setup for smooth sine wave simulation.

kinematic viscosity	$\nu \in \{100, 10, 1\}$
slip length	$\lambda \in \{100, 10, 1\}$
temporal domain	$t \in [0, 2]$
spatial domain	periodic $x \in [-1, 1]$
spatial resolution	$n_x = 1000$
initial height	$h(x, 0) = 1 - 0.1 \sin\left(\frac{\pi x}{2}\right)^2$
initial velocity profile	$u(x, 0, \xi) = 0.5\xi$
CFL condition	0.7
numerical scheme	PRICE [4, 5]

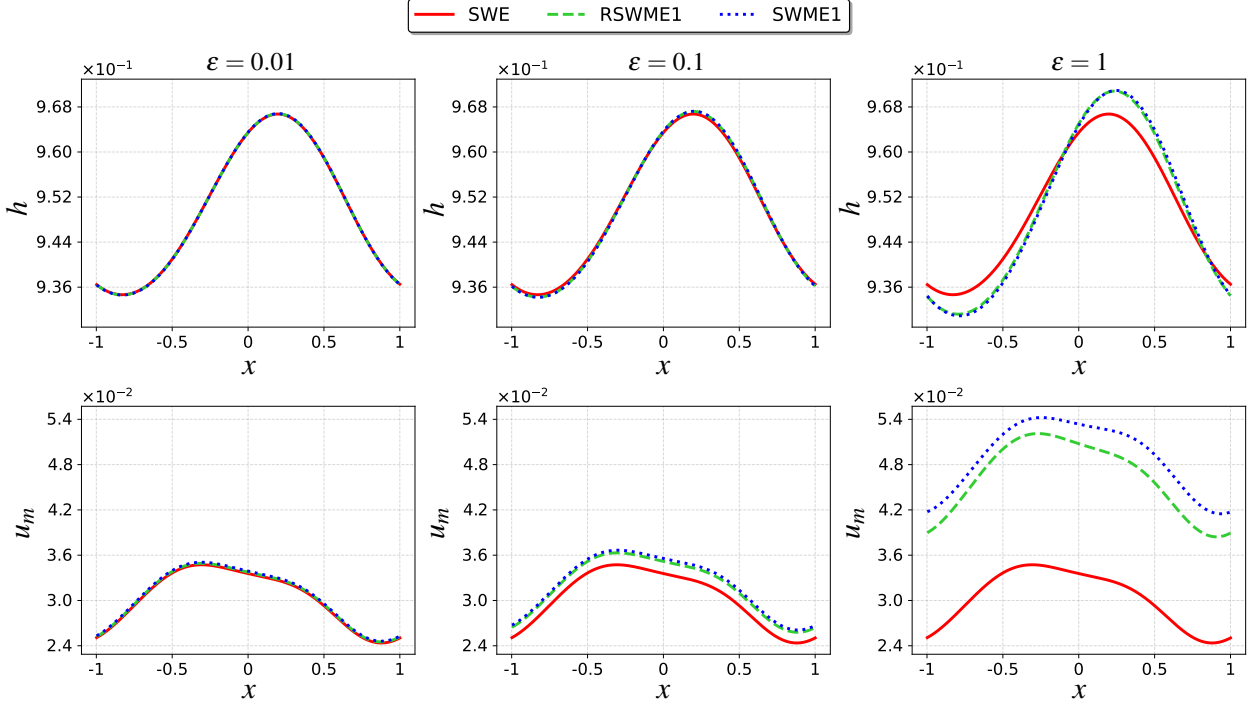


Figure 4: Smooth sine-wave test comparing the SWE (red, solid), RSWME1 (green, dashed), and SWME1 (blue, dotted) models at $t = 2.0$. The results are presented for the variables height h (top row) and average velocity u_m (bottom row) across three values of ε : $\varepsilon = 0.01$ (left), $\varepsilon = 0.1$ (middle), and $\varepsilon = 1$ (right).

h and average velocity u_m . Thus, the RSWME1 are more accurate than the SWE.

In Table 4, the relative L_1 -error for the RSWME1 and SWE solutions is shown with respect to the SWME1 as the reference solution. The results show that the RSWME1 provide a more accurate approximation of the SWME1 compared to the SWE. The smallest relative improvement of the RSWME1 over SWE when comparing their relative errors is 64%, which is observed in the variable u_m for $\varepsilon = 0.01$. The largest relative improvement of 88% occurs in variable h for $\varepsilon = 0.1$.

In Figure 5 the numerical solutions for the moment variable α_1 are shown. In this figure the erroneous peaks for $\varepsilon = 1$ shown in the sharp gradient case from Figure 2 are not present. Hence, for a test case with smaller gradients of h^4 the closure relations for the moment variables are accurate up to a larger value of ε .

For $N = 2$, we compare the RSWME2 system from (52) with the SWE and SWME2. Numerical tests for the smooth sine wave cases were again conducted for various values of ε over a duration of two seconds. In Figure 6, the numerical solutions for the average velocity u_m and height h are presented. In Figure 6 one can observe that the RSWME2 lead to a more accurate solution of the SWME2, compared to the SWE. In Table 5, the relative L_1 -error for the RSWME2 and SWE solutions are shown with respect to the SWME2 as the reference solution. The errors in Table 4 and Table 5 are of a similar magnitude. This indicates that for both

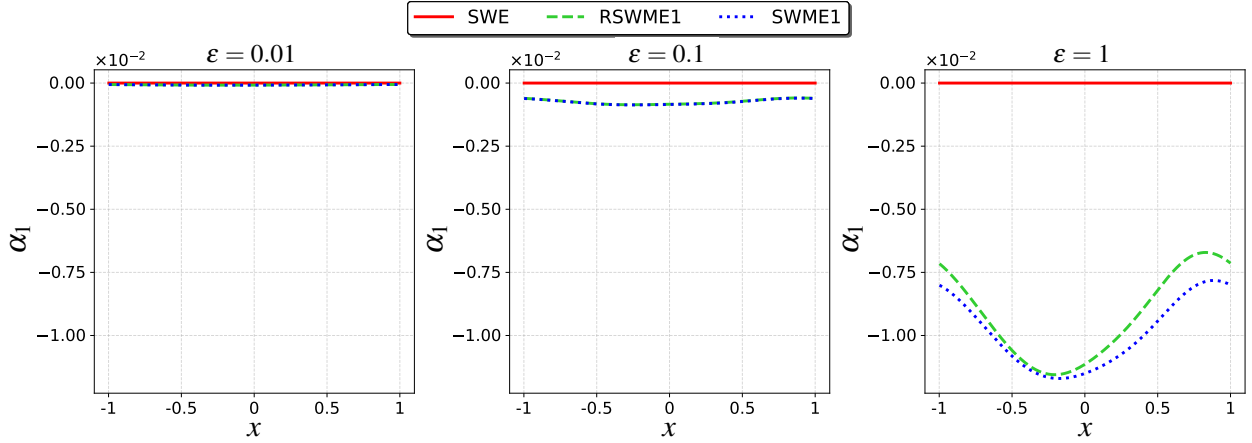


Figure 5: Smooth sine-wave test comparing the SWE (red, solid), RSWME1 (green, dashed), and SWME1 (blue, dotted) models at $t = 2.0$. The results are presented for the moment coefficient α_1 across three values of ε : $\varepsilon = 0.01$ (left), $\varepsilon = 0.1$ (middle), and $\varepsilon = 1$ (right).

$N = 1$ and $N = 2$, the RSWME lead to an approximation closer to the SWME2 compared to the SWE. The smallest relative improvement by selecting the RSWME2 over the SWE is 57% and occurs in variable u_m , when $\varepsilon = 0.01$. The largest relative improvement takes place when $\varepsilon = 1$ for 86% and is measured in h .

By substituting the numerical solutions for u_m and h into the closure relations (50) and (51), we reconstruct the moment variables α_1 and α_2 in the RSWME2 system. The $\partial_x(h^4)$ -term in (50)-(51) is numerically computed using a Godunov FVM scheme. In Figure 7, the moment variables from the RSWME2 framework are presented alongside the numerically computed SWME2 moment variables. For $\varepsilon = 0.01$, the values of α_1 and α_2 in both the RSWME2 and SWME2 frameworks vanish and remain close to zero. For $\varepsilon = 0.1$, the values of α_1 and α_2 deviate further from zero compared to smaller values of ε . Notably, for $\varepsilon = 0.1$, the RSWME2 and SWME2 solutions for α_1 and α_2 coincide. For $\varepsilon = 1$, the approximated RSWME2 values of α_1 and α_2 lie between the SWME2 values and the zero moment value for the SWE. Additionally, for $\varepsilon = 0.1$ and $\varepsilon = 1$, the SWME2 and RSWME2 solutions for α_2 are consistently smaller than those for α_1 .

Comparison of RSWME2 and HRSWME2 Using the configuration of Table 3, we perform numerical tests for $N = 2$ comparing the RSWME2 and the HRSWME2 from Theorem 2 for various values of $\varepsilon = 0.1, 1, 10$. In Table 6, the errors for the numerical tests experiments are presented, with the SWME2 serving as the reference solution.

For the values of $\varepsilon = 0.1, 1$, we can observe that the differences between the RSWME2 and HRSWME2 in terms of error are not significant. There are two reasons for this. First, the RSWME2 model is stable, since ε is not too large and thereby the condition (58) holds. Second, because $h < 1$ holds in Figure 6, the hyperbolicity condition $0 < h < 1 < \frac{3\sqrt{5}}{\varepsilon}$, is satisfied for $\varepsilon = 0.1, 1$.

In Theorem 2, the added hyperbolic regularisation term is of order $\mathcal{O}(\varepsilon^4)$. For $\varepsilon = 0.1$, this term is negligible due to its small magnitude. Furthermore, the friction term is scaled by a factor of $\frac{4}{6.180^2} \approx 2 \times 10^{-5}$, which means that its contribution is minimal. Consequently, even for $\varepsilon = 1$, the additional term remains small.

Table 4: Relative L_1 -error ($t = 2.0$ and $N = 1$) for the smooth sine wave test.

	$\varepsilon = 0.01$	$\varepsilon = 0.1$	$\varepsilon = 1$
SWE, in h	4.6365e-5	3.6815e-4	3.2456e-3
RSWME1, in h	1.7695e-5	5.4793e-5	4.3920e-4
SWE, in u_m	9.4071e-3	5.8338e-2	3.8118e-1
RSWME1, in u_m	4.0201e-3	1.0659e-2	5.6338e-2

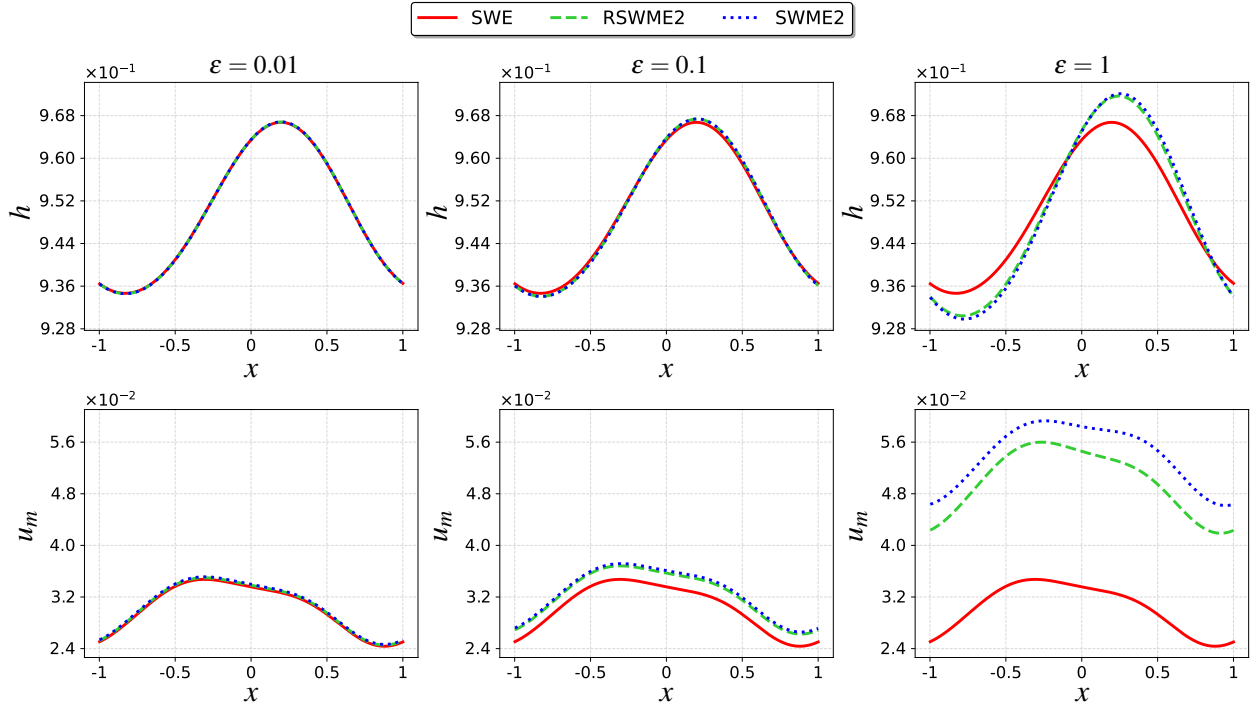


Figure 6: Smooth sine-wave test comparing the SWE (red, solid), RSWME2 (green, dashed), and SWME2 (blue, dotted) models at $t = 2.0$. The results are presented for the variables height h and average velocity u_m across three values of ε : $\varepsilon = 0.01$ (left), $\varepsilon = 0.1$ (middle), and $\varepsilon = 1$ (right).

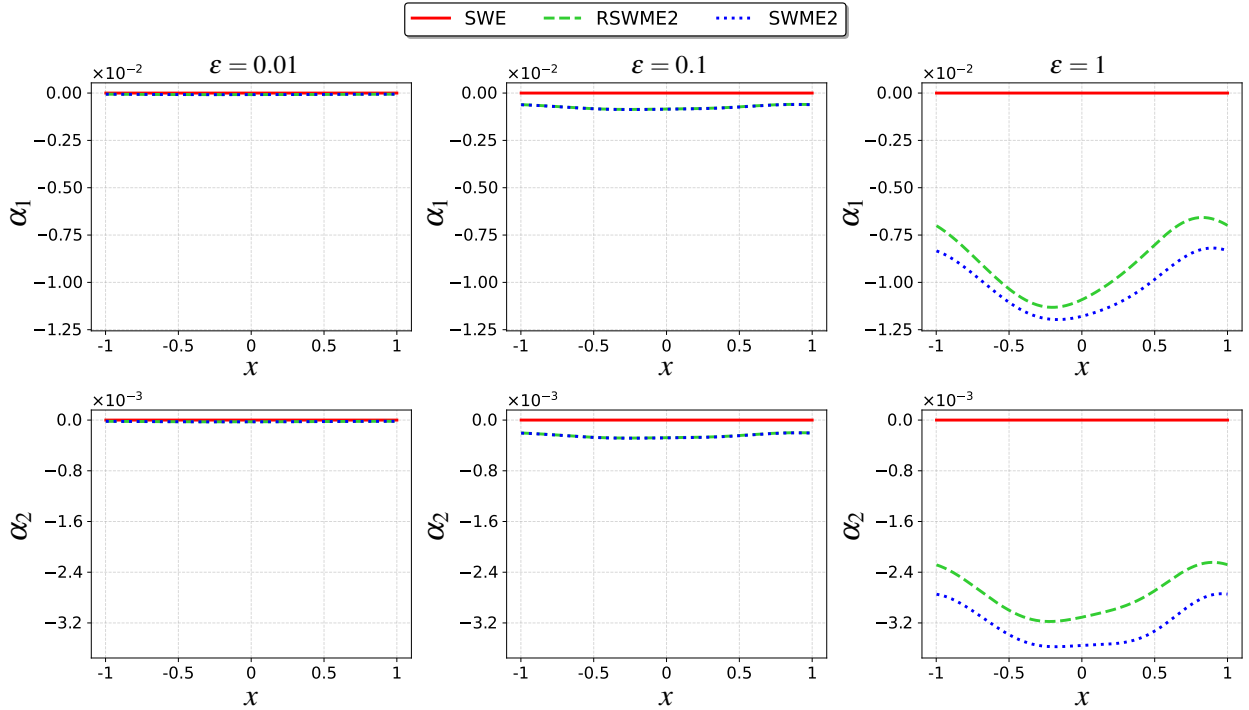


Figure 7: Smooth wave test comparing the SWE (red, solid), RSWME2 (green, dashed), and SWME2 (blue, dotted) models at $t = 2.0$. The results are presented for the moment coefficients α_1 and α_2 across three values of ε : $\varepsilon = 0.01$ (left), $\varepsilon = 0.1$ (middle), and $\varepsilon = 1$ (right).

Given that the added regularisation term is negligible for both $\varepsilon = 0.1$ and $\varepsilon = 1$, the difference between the solutions for RSWME2 and HRSWME2 can be expected to be insignificant.

For the largest value of $\varepsilon = 10$ in the numerical test, the HRSWME2 exhibit smaller errors compared

Table 5: Relative L_1 -error ($t = 2.0, N = 2$) for the smooth sine wave test.

	$\varepsilon = 0.01$	$\varepsilon = 0.1$	$\varepsilon = 1$
SWE, in h	5.6009e-5	4.7676e-4	4.1328e-3
RSWME2, in h	1.6798e-5	5.5410e-5	6.1433e-4
SWE, in u_m	1.1182e-2	7.2932e-2	4.3821e-1
RSWME2, in u_m	4.0137e-3	1.0549e-2	7.4865e-2

Table 6: The relative L_1 -error ($t = 2.0, N = 2$) for the sine wave test.

	$\varepsilon = 0.1$	$\varepsilon = 1$	$\varepsilon = 10$
SWE, in h	4.7676e-4	4.1328e-3	1.6712e-2
RSWME2, in h	5.5410e-5	6.1433e-4	3.5656e-1
HRSWME2, in h	5.5410e-5	6.1407e-4	3.6133e-2
SWE, in u_m	7.2932e-2	4.3821e-1	8.2080e-1
RSWME2, in u_m	1.0549e-2	7.4865e-2	1.5482e-0
HRSWME2, in u_m	1.0549e-2	7.4790e-2	1.0000e-1

to the RSWME2. Importantly, at $\varepsilon = 10$, the condition in (58) no longer holds. This potential breakdown of hyperbolicity of the RSWME2 can introduce instabilities, resulting in erroneous solutions. Consequently, the inclusion of a hyperbolicity term in the HRSWME2 helps to mitigate these instabilities, which explains its improved accuracy.

On the other hand, for $\varepsilon = 10$ the errors of the SWE are smaller than for both the HRSWME2 and RSWME2. This can be explained by the fact that a core model assumption no longer holds, which states that ε is small. Hence, the HRSWME2, while hyperbolic in comparison to the RSWME2, are no longer valid for $\varepsilon = 10$.

In further tests we will not continue to use the HRSWME2 model since for valid values of ε we see no improvement in accuracy or in stability. Whereas accuracy gains are observed for large ε values, the underlying assumptions of the RSWME2 model break down. In this situation, which also results in larger errors for the HRSWME2 compared to the SWE model. Consequently, introducing a hyperbolic regularisation term to the HRSWME2 does not yield any benefit for the numerical solution.

4.4 Test III: square root velocity profile

To investigate whether increasing the number of moments results in a more accurate approximation, we select an initial velocity profile from [10] with a square root $u(x, \zeta, t) = \frac{2}{3} \sqrt{\zeta}$. The initial conditions for the average velocity and the first moment coefficients are

$$u_m(x, 0) = 1, \quad \alpha_1(x, 0) = -\frac{3}{5}, \quad \alpha_2(x, 0) = -\frac{1}{7},$$

$$\alpha_3(x, 0) = -\frac{1}{15}, \quad \alpha_4(x, 0) = -\frac{3}{77}, \quad \alpha_5(x, 0) = -\frac{3}{35}, \quad \alpha_6(x, 0) = \frac{1}{55}.$$

In Table 7, the configurations for the numerical tests are shown.

Table 7: Numerical setup for the square root velocity test.

kinematic viscosity	$\nu = 2$
slip length	$\lambda = 2$
temporal domain	$t \in [0, 2]$
spatial domain	periodic $x \in [-1, 1]$
spatial resolution	$n_x = 1000$
initial height	$h(x, 0) = 1 - 0.1 \sin\left(\frac{\pi x}{2}\right)^2$
initial velocity profile	$u(x, 0, \zeta) = \frac{2}{3} \sqrt{\zeta}$
CFL condition	0.7
numerical scheme	PRICE [4, 5]

Various numerical tests are performed for $N = 2, 4, 6$ to compare the accuracy for the SWME, RSWME and SWE solutions. It is important to note that according to Theorem 3, the RSWME2, the RSWME4 and the RSWME6 are identical. In Figure 8, the numerical solutions for the average velocity u_m and height h are presented. For every choice of $N = 2, 4, 6$, the RSWME model is closer to the the SWME model for both h and u_m compared to the SWE model.

By substituting the numerical solutions for u_m and h into the closure relation (75) we reconstruct the moment variables $\alpha_{N,i}$, $i = 1, \dots, N$, in the RSWME system. The $\partial_x(h^4)$ -term in (75) is again numerically computed using a Godunov FVM scheme.

In Figure 9, the moment variables from the RSWME framework are presented alongside the numerically computed SWME moment variables. We observe that the magnitude of $\alpha_{N,i}$, $i = 1, \dots, N$, decreases strictly as we increase the order of the moments. This makes sense, because the $\alpha_{N,i}$, for $i = 1, \dots, N$, are expansion coefficients of a converging expansion.

Computations for α_5 and α_6 show that the coefficients for the RSWME are already equal to zero, which goes into the same direction as the SWME, for which a small contribution of the size of $\mathcal{O}(10^{-7})$ - $\mathcal{O}(10^{-8})$ remains. Furthermore, one can observe that for $N = 2, 4, 6$, the RSWME moment closure relations yield solutions for $\alpha_{N,i}$ (where $i \leq 4$) that provide a more accurate approximation of the SWME solutions compared to the case where $\alpha_{N,i} = 0$, for $i = 1, \dots, N$ in the SWE framework.

By employing the numerically computed solutions for u_m and the moment variables, the vertical velocity profile at $x = x_0 = 0.5$ can be visualised using the relation provided in (3). In Figure 10, we compare the velocity profiles for the SWE, SWME and RSWME for $N = 2, 4, 6$, with the fixed constant $\varepsilon = 0.5$. The vertical velocity profile predicted by the RSWME aligns more closely with that of the SWME than does the profile obtained from the SWE. For every choice of $N = 2, 4, 6$ the RSWME approximates the SWME better, compared to the SWE.

In Table 8, the computational runtimes for the various models are presented. The differences in runtimes between the SWE and RSWME are comparatively negligible. However, we can observe that for $N = 2, 4, 6$, the runtime for the SWME is always significantly larger compared to the SWE and RSWME. This can be explained by the fact that the SWE and RSWME solve a system for only 2 variables, whereas the SWME solve a system for $N + 2$ variables.

The small difference in runtime between the RSWME and SWE arises from an additional post-processing step required for the RSWME: computing the closure relations for the moment variables (75). In the numer-

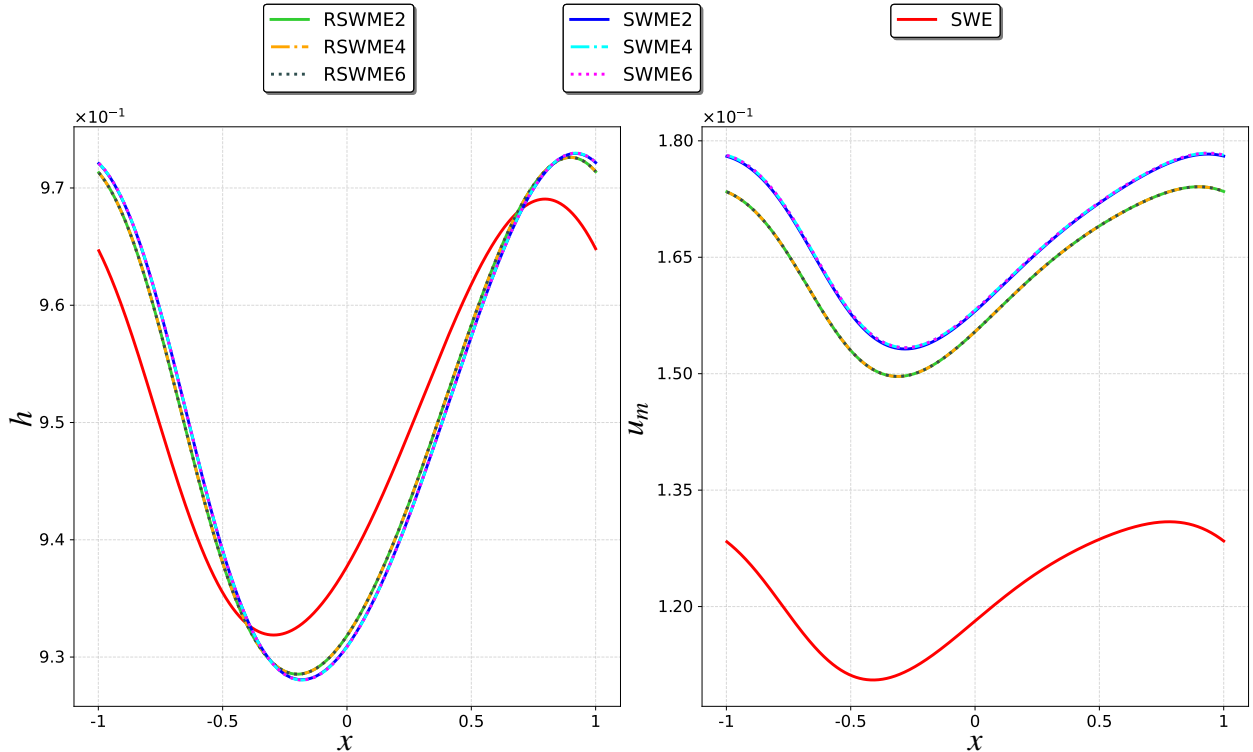


Figure 8: Square root velocity profile test comparing the SWE, RSWME, and SWME models for $N = 2$ (solid), $N = 4$ (dashed) and $N = 6$ (dotted) at $t = 2.0$. The results are presented for the variables height h (left) and average velocity u_m (right) and $\varepsilon = 0.5$.

Table 8: Comparison of CPU runtime for simulating the square root velocity profile test case up to $t = 2$ on AMD EPYC 7763 64-core processor.

N	SWE (s)	SWME (s)	RSWME (s)
0	132.6	-	-
2	-	170.0	138.7
4	-	307.4	138.6
6	-	606.8	138.9

ical test, results are computed up to $t = 2$, and the closure relations for the moment variable are evaluated only once at the final time step.

Our experimental results in Table 8 indicate that the RSWME model is between 18% (for $N = 2$) and 77% (for $N = 6$) faster than the SWME. The simulation time of the RSWME2 exceeds the runtime of the SWE by a mere 5%, which is an insignificant amount of overhead. Furthermore, our results show that increasing the number of moments significantly raises the simulation time for the SWME model, whereas the simulation time for the RSWME remains unchanged.

For conciseness, the runtimes for the test cases with a sharp wave and a smooth sine wave are not included. During experiments, we noticed similar speedups as in Table 8.

5 Conclusion

In this paper we introduced the Reduced Shallow Water Moment Equations (RSWME), as an accurate but more efficient approximation of Shallow Water Moment Equations (SWME) with high viscosity and large slip length. The RSWME are able to model vertical velocity profiles with slight deviations from a uniform velocity profile, while having fewer variables compared to the SWME.

A notable cost of the SWME lies in its need to include a larger number of variables compared to the

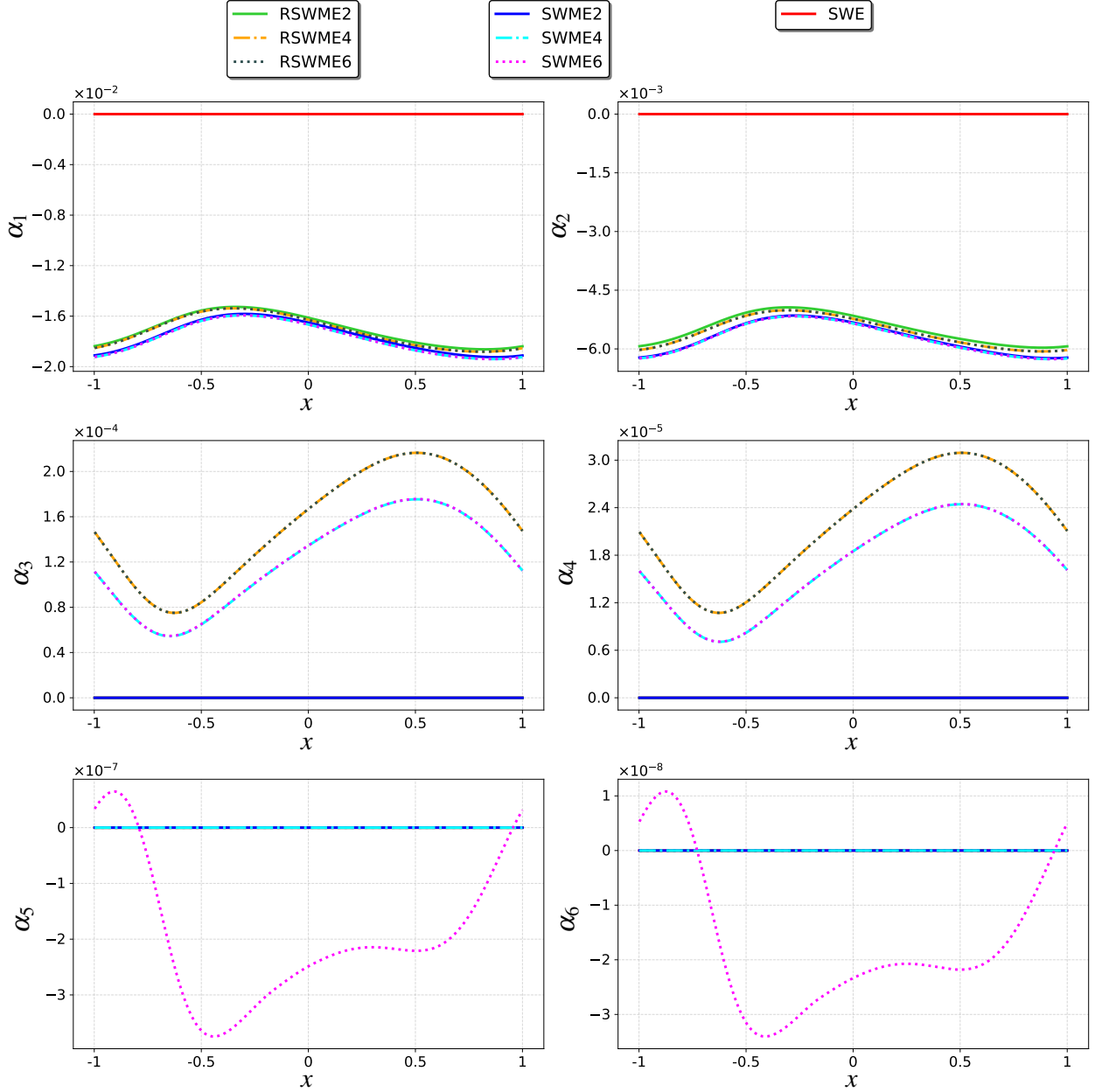


Figure 9: Square root velocity profile test comparing the SWE, RSWME, and SWME models for $N = 2$ (solid), $N = 4$ (dashed) and $N = 6$ (dotted) at $t = 2.0$. The results are presented for the moment coefficient $\alpha_{N,i}$, $i = 1, \dots, 6$ and $\varepsilon = 0.5$.

Shallow Water Equations (SWE), even when the SWME have an equilibrium that could be represented by fewer variables. To simplify the SWME near an equilibrium where viscosity and slip length are large, we apply an asymptotic expansion to analyse small deviations around this equilibrium.

The SWME were subjected to a large-viscosity and large-slip scaling. Applying asymptotic analysis to this SWME model yielded explicit closure relations for moment variables up to second order in the smallness parameter. The RSWME were obtained by substituting these closure relations into the original SWME model. Because the RSWME are a dimensionally reduced model and contain fewer variables, the RSWME have a lower computational cost. Additionally, we showed that the closed RSWME system is identical for large numbers of moments.

The simple and closed form allowed for an in-depth analysis of the equations, which was exemplified by studying its hyperbolicity. Similar to related SWME models, a hyperbolic regularisation was performed.

The accuracy and computational efficiency of the RSWME were evaluated through numerical tests in-

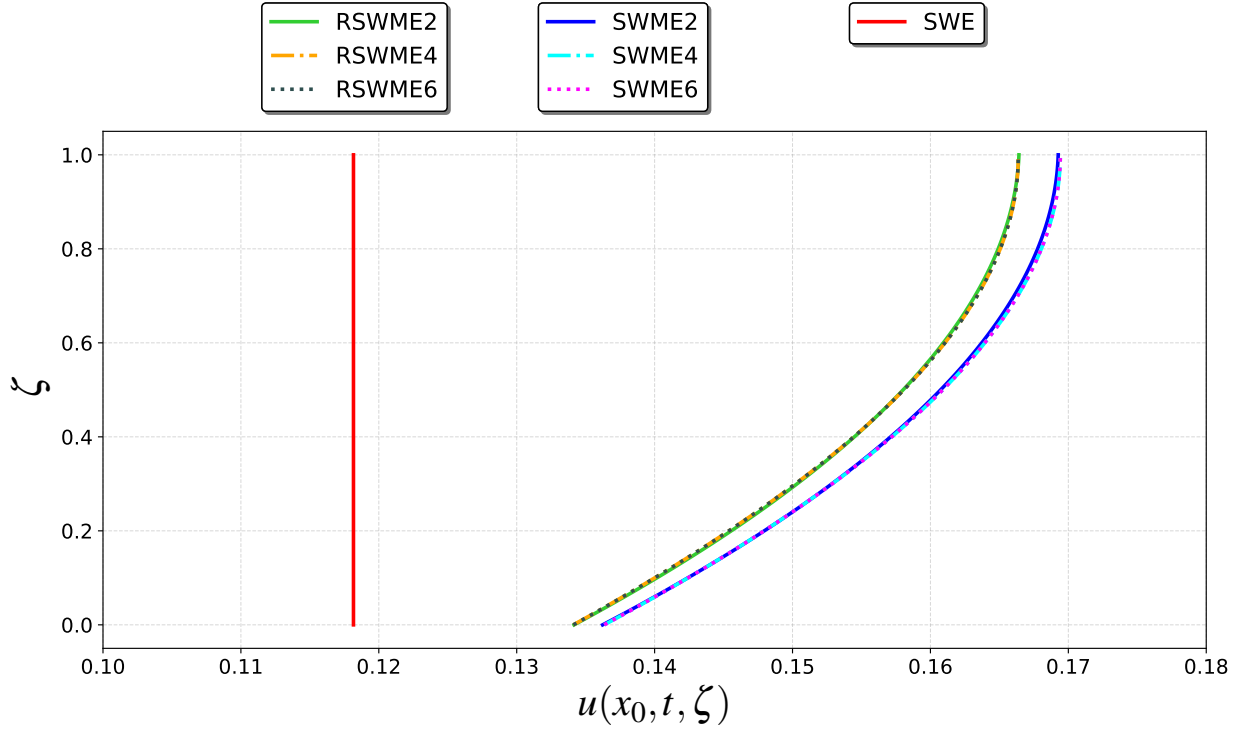


Figure 10: Square root velocity profile test comparing the SWE, RSWME, and SWME models for $N = 2$ (solid), $N = 4$ (dashed) and $N = 6$ (dotted) at $t = 2.0$. The results are presented for the vertical velocity profile $u(x_0, t, \zeta)$ for $\varepsilon = 0.5$ and $x_0 = 0.0$.

volving a wave with a sharp height gradient, a smooth sine wave test case, and a square root initial velocity distribution. While showing remarkable accuracy for the height and average velocity, the test with a wave and a sharp gradient of height yields incorrect solutions in the moment variables for large deviations from equilibrium. For smooth sine waves, accurate RSWME solutions were obtained that approximate the SWME more accurately compared to the SWE, for both small and large deviations from equilibrium. In the smooth sine wave test the relative error of the RSWME improves by up to 88% relatively compared to the SWE. A test with a square root velocity profile showed that the RSWME yield a more accurate velocity profile than the SWE. For the square root velocity profile test, the RSWME model demonstrates a runtime reduction up to 77%, compared to the SWME.

These findings support two distinct interpretations: (1) The RSWME achieve accuracy comparable to the SWME while requiring significantly lower computational time, and; (2) The RSWME model outperforms the SWE in accuracy with similar computational costs. These outcomes render the RSWME model efficient for simulations.

For future work, the application of asymptotic approximations to SWME with alternative scalings for viscosity and slip length are of interest. Such an analysis could focus on the equilibria detailed in [A](#), by developing for example reduced models characterised by a small slip length.

CRedit authorship contribution statement

M. Daemen: Conceptualization, Methodology, Software, Formal Analysis, Investigation, Data Curation, Writing - Original Draft, Writing - Review & Editing, Visualization. **J. Careaga:** Conceptualization, Writing - Review & Editing, Supervision, Visualization. **Z. Cai** Conceptualization, Resources, Writing - Review & Editing. **J. Koellermeier:** Conceptualization, Resources, Writing - Review & Editing, Supervision, Funding acquisition.

Acknowledgments

This work is supported by the Dutch Research Council (NWO) through the ENW Vidi project HiWAVE with file number VI.Vidi.233.066. We acknowledge Rik Verbiest for providing a numerical simulation code for the Shallow Water Moment Equations (SWME).

Declaration of generative AI and AI-assisted technologies in the manuscript preparation process.

During the preparation of this work the author(s) used Le Chat from Minstral AI to improve writing style, improve formatting of equations and debug software. After using this tool/service, the author(s) reviewed and edited the content as needed and take(s) full responsibility for the content of the published article.

A Asymptotic approximations for alternative scalings of friction parameters

For different scalings of the friction parameters λ and ν , approximations near their respective equilibria can be derived. Table 9 summarises the feasible cases, demonstrating that such approximations can only be obtained when the viscosity ν is of order $\mathcal{O}(\varepsilon^{-1})$ or the slip length λ is of order $\mathcal{O}(\varepsilon)$. In this table the fourth column indicates the order of the asymptotic solution, while the fifth column lists the variables retained in the dimensionally reduced system near equilibrium.

A possible strategy, presented as case II, to reduce the number of variables involves scaling the slip length by $\lambda = \lambda_0 \varepsilon$. In the no-slip case II, the leading order solution as $\varepsilon \rightarrow 0$ in (7b) and (7c) reduces to

$$u_m + \alpha_1 + \dots + \alpha_N = 0. \quad (85)$$

This leading order approximation (85) coincides with the no-slip boundary condition, $u|_{\xi=0} = 0$. In the no-slip case II, an asymptotic approximation exists, but reduces the system only by a single variable through the approximation of α_N as a function of h , u_m , and $\alpha_1, \dots, \alpha_{N-1}$, resulting in approximations of order $\mathcal{O}(\varepsilon^0)$. To study a case that achieves greater dimensional reduction and more accurate asymptotic approximations, we focus on the viscous slip case in our research.

In cases III and IV in Table 9, the scalings $\nu = \frac{\lambda_0}{\varepsilon}$ and $\nu = \frac{\lambda_0}{\varepsilon}$, $\lambda = \lambda_0 \varepsilon$ are applied, respectively. Letting $\varepsilon \rightarrow 0$ in (7a)-(7c), results in the leading order equations

$$u_m = \alpha_1 = \dots = \alpha_N = 0, \quad \partial_t h = 0. \quad (86)$$

For cases III and IV, the application of asymptotic approximations ultimately produces a system reduced to one variable h . Additionally, the approximated solutions for u_m and α_j ($j = 1, \dots, N$) are of order $\mathcal{O}(\varepsilon)$, indicating that these solutions are already close to a steady-state equilibrium where h is constant and $u = 0$.

Table 9: Possible scalings for slip length λ and viscosity ν .

Case	λ	ν	Order of solution	Variables for \mathcal{E}
I	$\mathcal{O}(\varepsilon^{-1})$	$\mathcal{O}(\varepsilon^{-1})$	$\mathcal{O}(\varepsilon^2)$	h, u_m
II	$\mathcal{O}(\varepsilon)$	$\mathcal{O}(\varepsilon^0)$	$\mathcal{O}(\varepsilon^0)$	$h, hu_m, h\alpha_1, \dots, h\alpha_{N-1}$
III	$\mathcal{O}(\varepsilon^0)$	$\mathcal{O}(\varepsilon^{-1})$	$\mathcal{O}(\varepsilon^3)$	h
IV	$\mathcal{O}(\varepsilon)$	$\mathcal{O}(\varepsilon^{-1})$	$\mathcal{O}(\varepsilon^3)$	h

B Proof of Theorem 3

In this section, we prove Theorem 3. First, we present Lemma 1 that explains how $C_N \mathbf{b} = 1$, can be solved for arbitrary N . Using Lemma 1, Theorem 3 is proven.

Lemma 1. Let $N \geq 2$ and $C_N \in \mathbb{R}^{N \times N}$ be the matrix with entries given by the constants $C_{Nij} = C_{ij}$ for $i, j = 1, \dots, N$ defined in (10), and let $\mathbf{1} \in \mathbb{R}^N$ be the vector of ones. Then, the following linear system

$$C_N \mathbf{b}_N = \mathbf{1}, \quad (87)$$

has a unique solution $\mathbf{b}_N = (b_1, b_2, \dots, b_N)^T \in \mathbb{R}^N$ given by

$$b_1 = \frac{1}{4}, \quad b_2 = \frac{1}{12}, \quad \text{and} \quad b_i = 0 \quad \text{for } i = 3, \dots, N.$$

Proof. We first observe that the matrix C_N can be computed component-wise as

$$C_{Nij} = C_{ij} = \begin{cases} 0 & \text{if } i - j \text{ is odd,} \\ 2 \min(i, j)(\min(i, j) + 1) & \text{if } i - j \text{ is even,} \end{cases} \quad (88)$$

for $i, j = 1, \dots, N$, according to [8]. From (88) we can readily observe that its first and second columns of C_N are the respective vectors

$$\begin{aligned} \mathbf{c}_1 &= (4, 0, 4, 0, 4, \dots)^T \in \mathbb{R}^N, \\ \mathbf{c}_2 &= (0, 12, 0, 12, 0, \dots)^T \in \mathbb{R}^N. \end{aligned}$$

Moreover, multiplying matrix C_N times $\mathbf{b}_N = (1/4, 1/12, 0, 0, \dots, 0)^T \in \mathbb{R}^N$ gives

$$C_N \mathbf{b}_N = \frac{1}{4} \mathbf{c}_1 + \frac{1}{12} \mathbf{c}_2 = \mathbf{1}.$$

Thus, \mathbf{b}_N is a solution to system (87), and because C_N is invertible, this solution also corresponds to the unique solution to (87). \square

A direct consequence of Lemma 1 is the equality

$$\tilde{B}_j^{(N)} = \sum_{k=1}^N (C_N^{-1})_{jk} = (C_N^{-1} \mathbf{1})_j = b_j, \quad \text{for } j = 1, \dots, N, \quad (89)$$

therefore $\tilde{B}_j^{(N)} = 0$ for $j = 3, \dots, N$, for all $N > 2$. In addition, we can immediately show that the vector $\tilde{\mathbf{b}}_N = (\frac{1}{3}b_1, \frac{1}{5}b_2, 0, 0, \dots)^T \in \mathbb{R}^N$ satisfies

$$\tilde{C}_N^T \tilde{\mathbf{b}}_N = \mathbf{1} \quad \text{equivalently} \quad \tilde{\mathbf{b}}_N = (\tilde{C}_N^T)^{-1} \mathbf{1} = (\tilde{C}_N^{-1})^T \mathbf{1}. \quad (90)$$

With the help of Lemma 1 we now prove Theorem 3.

Theorem 3 (Identical closed RSWME systems). *For $N \geq 2$, all RSWME systems are identical.*

Proof. To establish that the RSWME systems from (76) are identical for all $N \geq 2$, it suffices to demonstrate that the system matrix A^N from (77) and the source term S^N from (79) satisfy: $A^N(U) = A^2(U)$ and $S^N(U) = S^2(U)$ for all $N \geq 2$. Moreover, by their definitions, these equalities hold if and only if the following equalities are satisfied:

$$\Gamma^N = \Gamma^2, \quad \Phi^N = \Phi^2, \quad \Omega^N = \Omega^2, \quad \Lambda^N = \Lambda^2, \quad \text{for } N \geq 2,$$

where $\Gamma^N, \Phi^N, \Omega^N$ and Λ^N are defined in (78) and (80). Using (89), and the fact that $\tilde{B}_j^{(N)} = 0$ for all $j \geq 3$ and arbitrary $N > 2$, we can directly conclude that

$$\Gamma^N = \sum_{j=1}^N \frac{(\tilde{B}_j^{(N)})^2}{2j+1} = \frac{(\tilde{B}_1^{(N)})^2}{3} + \frac{(\tilde{B}_2^{(N)})^2}{5} = \frac{(\tilde{B}_1^{(2)})^2}{3} + \frac{(\tilde{B}_2^{(2)})^2}{5} = \Gamma^2,$$

and

$$\Omega^N = \sum_{j=1}^N \tilde{B}_j^{(N)} = \tilde{B}_1^{(N)} + \tilde{B}_2^{(N)} = \tilde{B}_1^{(2)} + \tilde{B}_2^{(2)} = \Omega^2.$$

On the other hand, we define the matrix $P_N = \tilde{C}_N^{-1} C_N^{-1}$ where each entry is denoted as $(P_N)_{ij} = P_{Nij}$ for all $i, j = 1, \dots, N$. Subsequently, by Lemma 1 and Equation (90), it follows that

$$\begin{aligned} \Phi^N &= \sum_{i=1}^N \sum_{j=1}^N P_{Nij} = \mathbf{1}^T (P_N \mathbf{1}) = \mathbf{1}^T (\tilde{C}_N^{-1} (C_N^{-1} \mathbf{1})) \\ &= \mathbf{1}^T (\tilde{C}_N^{-1} \mathbf{b}_N) = ((\tilde{C}_N^{-1})^T \mathbf{1})^T \mathbf{b}_N = (\tilde{\mathbf{b}}_N)^T \mathbf{b}_N = \frac{1}{3} b_1^2 + \frac{1}{5} b_2^2 \\ &= \mathbf{1}^T (\tilde{C}_2^{-1} C_2^{-1} \mathbf{1}) = \Phi^2. \end{aligned}$$

Finally, expressing Λ^N in terms of Φ^N and Ω^N yields

$$\Lambda^N = -\Phi^N + (\Omega^N)^2 = -\Phi^2 + (\Omega^2)^2 = \Lambda^2,$$

thereby concluding the proof. □

References

- [1] D. Arcas and Y. Wei. Evaluation of velocity-related approximations in the nonlinear shallow water equations for the Kuril Islands, 2006 tsunami event at Honolulu, Hawaii. *Geophysical Research Letters*, 38(12), 2011.
- [2] M. Bauerle, A. J. Christlieb, M. Ding, and J. Huang. On the Rotational Invariance and Hyperbolicity of Shallow Water Moment Equations in Two Dimensions. *SIAM Journal on Mathematical Analysis*, 57(1):1039–1085, 2025.
- [3] A. V. Bobylev. Instabilities in the Chapman-Enskog Expansion and Hyperbolic Burnett Equations. *Journal of Statistical Physics*, 124(2–4):371–399, December 2005.
- [4] A. Canestrelli, A. Siviglia, M. Dumbser, and E.F. Toro. Well-balanced high-order centred schemes for non-conservative hyperbolic systems. Applications to shallow water equations with fixed and mobile bed. *Advances in Water Resources*, 32(6):834–844, June 2009.
- [5] M. J. Castro Díaz and E. Fernández-Nieto. A class of computationally fast first order finite volume solvers: Pvm methods. *SIAM Journal on Scientific Computing*, 34(4):A2173–A2196, January 2012.
- [6] S. Chapman and T.G. Cowling. *The Mathematical Theory of Non-Uniform Gases*. Cambridge University Press, Cambridge, 3 edition, 1990.
- [7] J. Garres-Díaz, M.J. Castro Díaz, J. Koellermeier, and T. Morales de Luna. Shallow Water Moment Models for Bedload Transport Problems. *Communications in Computational Physics*, 30(3):903–941, 2021.
- [8] Q. Huang, J. Koellermeier, and W.-A. Yong. Equilibrium stability analysis of hyperbolic shallow water moment equations. *Mathematical Methods in the Applied Sciences*, 45(10):6459–6480, 2022.
- [9] J. Koellermeier. A new Energy Equation Derivation for the Shallow Water Linearized Moment Equations. Ghent, Belgium, September 2025. Universiteit Gent. to appear in *Book of Abstracts of the 9th International Conference on Advanced Computational Methods in Engineering and Applied Mathematics (ACOMEN2025)*.

- [10] J. Koellermeier and E. Pimentel-García. Steady states and well-balanced schemes for shallow water moment equations with topography. *Applied Mathematics and Computation*, 427:127166, 2022.
- [11] J. Koellermeier and M. Rominger. Analysis and Numerical Simulation of Hyperbolic Shallow Water Moment Equations. *Communications in Computational Physics*, 28(3):1038–1084, 2020.
- [12] J. Kowalski and M. Torrilhon. Moment Approximations and Model Cascades for Shallow Flow. *Communications in Computational Physics*, 25(3):669–702, 2019.
- [13] G.M. Kremer. The Methods of Chapman-Enskog and Grad and Applications. Technical Report RTO-EN-AVT-194, NATO Research and Technology Organisation, 2006.
- [14] D. Liang. Evaluating shallow water assumptions in dam-break flows. *Proceedings of the Institution of Civil Engineers - Water Management*, 163(5):227–237, 2010.
- [15] J. A. Liggett. Critical Depth, Velocity Profiles, and Averaging. *Journal of Irrigation and Drainage Engineering*, 119(2):416–422, 1993.
- [16] R. N. Miller. *Numerical Modeling of Ocean Circulation*, page 35–86. Cambridge University Press, 2007.
- [17] M. Sanz-Ramos, E. Bladé, P. Oller, and G. Furdada. Numerical modelling of dense snow avalanches with a well-balanced scheme based on the 2D shallow water equations. *Journal of Glaciology*, 69(278):1646–1662, 2023.
- [18] U. Scholz, J. Kowalski, and M. Torrilhon. Dispersion in Shallow Moment Equations. *Communications on Applied Mathematics and Computation*, 6(4):2155–2195, December 2023.
- [19] H. Struchtrup. *Macroscopic Transport Equations for Rarefied Gas Flows*. Springer-Verlag Berlin Heidelberg, 2005.
- [20] R. Verbiest and J. Koellermeier. Capturing Vertical Information in Radially Symmetric Flow Using Hyperbolic Shallow water Moment Equations. *Communications in Computational Physics*, 37(3):810–848, June 2025.
- [21] C.B. Vreugdenhil. Equations. In *Numerical Methods for Shallow-Water Flow*, pages 15–46. Springer Netherlands, Dordrecht, 1994.
- [22] D. Wang. Extensions and Simulations of Shallow Water Equations. Master’s thesis, National University of Singapore, Singapore, 2023.